iScience

CellPress
OPEN ACCESS

Article

Ethanol induces replication fork stalling and membrane stress in immortalized laryngeal cells

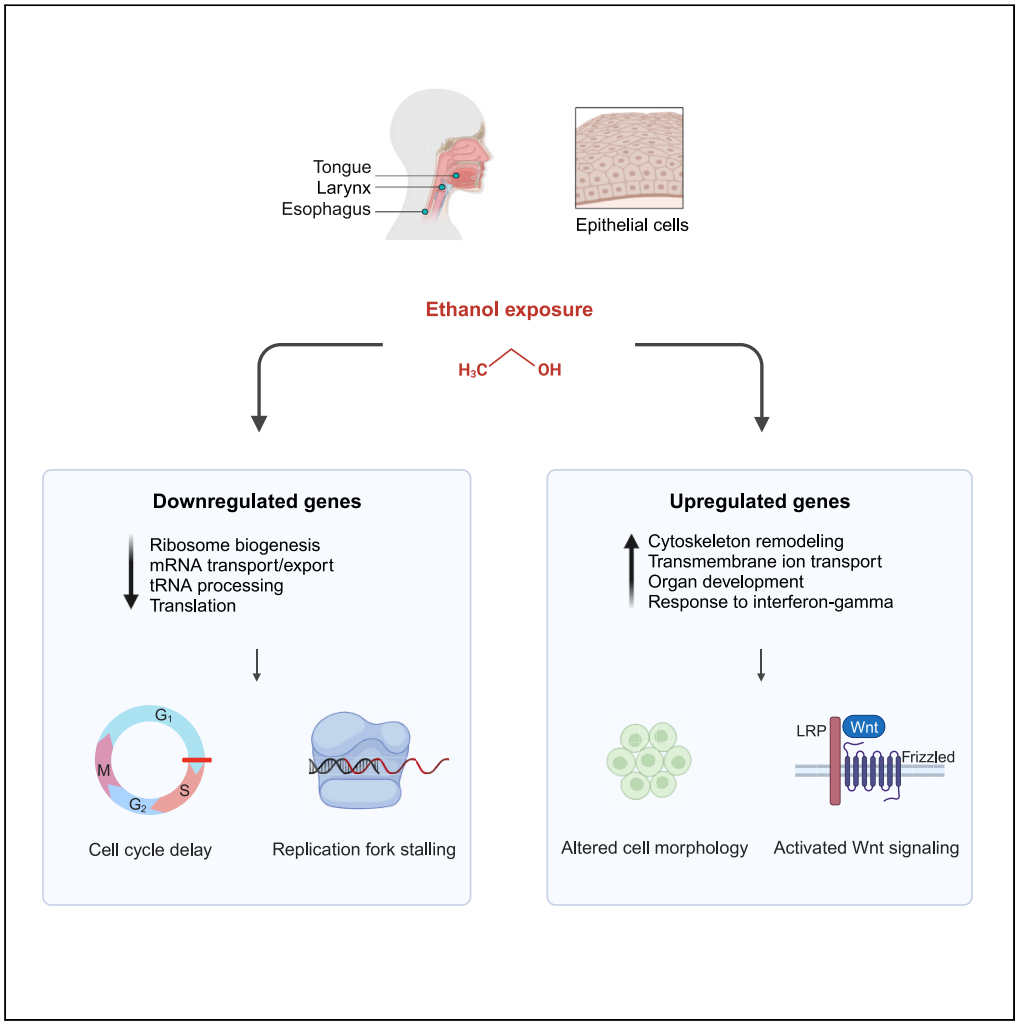

Lore Hoes, Karin Voordeckers, Rüveyda Dok, ..., Diether Lambrechts, Sandra Nuyts, Kevin J. Verstrepen

lore.hoes@kuleuven.be

Highlights

Ethanol exposure slows down cell cycle and replication fork progression

Ethanol exposure changes cellular morphology

Ethanol exposure results in the upregulation of Wnt signaling ligands and receptors

The pleiotropic effects of ethanol shed light on ethanol-related disease mechanisms

Hoes et al., iScience *26*, 108564
December 15, 2023
https://doi.org/10.1016/j.isci.2023.108564

iScience

CellPress
OPEN ACCESS

Article

Ethanol induces replication fork stalling and membrane stress in immortalized laryngeal cells

Lore Hoes,[1,2,3,*] Karin Voordeckers,[1,2] Rüveyda Dok,[3] Bram Boeckx,[4,5] Bart Steemans,[7] Diyavarshini Gopaul,[6] Philippe Pasero,[6] Sander K. Govers,[7] Diether Lambrechts,[4,5] Sandra Nuyts,[3,8,9,10] and Kevin J. Verstrepen[1,2,9]

SUMMARY

Although ethanol is a class I carcinogen and is linked to more than 700,000 cancer incidences, a clear understanding of the molecular mechanisms underlying ethanol-related carcinogenesis is still lacking. Further understanding of ethanol-related cell damage can contribute to reducing or treating alcohol-related cancers. Here, we investigated the effects of both short- and long-term exposure of human laryngeal epithelial cells to different ethanol concentrations. RNA sequencing shows that ethanol altered gene expression patterns in a time- and concentration-dependent way, affecting genes involved in ribosome biogenesis, cytoskeleton remodeling, Wnt signaling, and transmembrane ion transport. Additionally, ethanol induced a slower cell proliferation, a delayed cell cycle progression, and replication fork stalling. In addition, ethanol exposure resulted in morphological changes, which could be associated with membrane stress. Taken together, our data yields a comprehensive view of molecular changes associated with ethanol stress in epithelial cells of the upper aerodigestive tract.

INTRODUCTION

Alcohol consumption has been associated with numerous diseases, including cancer,[1] with an estimated number of 740,000 newly diagnosed alcohol-attributed cancer cases in 2020.[2] Epidemiological studies have identified causal relationships between alcohol intake and several types of cancer.[3–5] According to the International Agency for Research on Cancer, alcohol (ethanol) is a causal risk factor for cancers of the oral cavity, larynx, pharynx, esophagus, liver, colorectum, and female breast.[6] Head and neck cancers, i.e., oral cavity, larynx, and pharynx cancers combined, have a strong background in ethanol etiology, with around 70% of the cases associated with alcohol or tobacco abuse, or both.[7] Most tumors form at sites where tissues come into direct contact with ethanol, such as the mouth, upper throat, and esophagus. Additionally, the dose of ethanol plays an important role as cancer risk increases linearly with the number of drinks consumed daily.[8]

Although epidemiological data demonstrate a clear link between ethanol intake and cancer, the molecular mechanisms underlying the carcinogenic effect of ethanol at different sites are not yet fully elucidated. The effects of ethanol have mostly been linked to acetaldehyde and reactive oxygen species (ROS), which are produced during oxidative ethanol catabolism.[9] Increased levels of ROS can result in oxidative stress and DNA damage, by the direct oxidation of DNA base pairs or by lipid peroxidation.[10] Acetaldehyde can also directly react with DNA, resulting in mutagenic and carcinogenic adducts or interstrand DNA crosslinks.[4,10,11] The important role of acetaldehyde is further confirmed by individuals carrying the *ALDH2* rs671 allele. This mutant allele dramatically reduces ALDH2 enzyme activity, thereby increasing acetaldehyde accumulation, which in turn leads to increased risk for ethanol-induced head and neck, and esophageal cancers.[12,13] In addition, acetaldehyde-related mutational signatures have been observed in esophageal, hypopharyngeal, and head and neck tumors.[14–16]

Despite the pivotal role of acetaldehyde in some cancers, mutational signatures that show no direct link to acetaldehyde have been associated with alcohol consumption in esophageal and liver cancer as well.[14,17] Ethanol exposure has been shown to have pleiotropic effects on eukaryotic cells. For instance, ethanol exposure resulted in DNA damage,[11,18–21] altered DNA methylation patterns,[22] oxidative stress,[23] mitochondrial dysfunction,[24] proteotoxic stress,[25] and altered membrane fluidity.[26] Additionally, ethanol has been linked to promoting metastasis

[1]Laboratory for Systems Biology, VIB-KU Leuven Center for Microbiology, 3000 Leuven
[2]Laboratory of Genetics and Genomics, Centre for Microbial and Plant Genetics, KU Leuven, 3000 Leuven, Belgium
[3]Laboratory of Experimental Radiotherapy, Department of Oncology, KU Leuven, 3000 Leuven, Belgium
[4]Laboratory of Translational Genetics, VIB-KU Leuven Center for Cancer Biology, 3000 Leuven, Belgium
[5]Laboratory of Translational Genetics, Department of Human Genetics, KU Leuven, 3000 Leuven, Belgium
[6]Institute of Human Genetics, CNRS, University of Montpellier, 34396 Montpellier, France
[7]Laboratory of Microbial Systems Cell Biology, Department of Biology, KU Leuven, 3000 Leuven, Belgium
[8]Department of Radiation Oncology, Leuven Cancer Institute, University Hospital Leuven, 3000 Leuven, Belgium
[9]These authors contributed equally
[10]Lead contact
*Correspondence: lore.hoes@kuleuven.be
https://doi.org/10.1016/j.isci.2023.108564

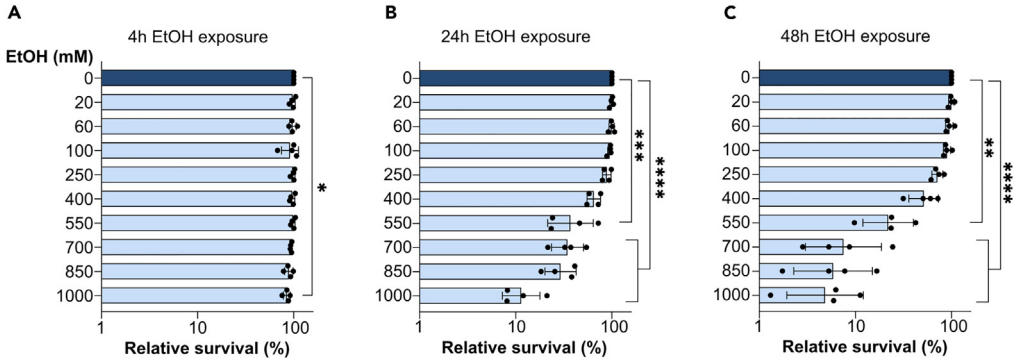

Figure 1. Ethanol affects cell survival in a dose- and time-dependent manner

(A–C) HuLa-PC cells were exposed to various ethanol (EtOH) concentrations for 4 h, 24 h, or 48 h. Survival was quantified relative to the control cells, treated with 0 mM ethanol, in every plate. Four independent biological replicates were measured and the bar indicates the average with standard deviation. Statistical significance was assessed by repeated-measures ANOVA with a Dunnett posthoc test calculated on log-transformed absorbance values. *$p < 0.05$, ***$p < 0.001$, ****$p < 0.0001$.

of cancer cells, probably by activating the epithelial to mesenchymal transition.[27–29] Lastly, ethanol can affect the oral microbiome. For instance, a recent study observed that laryngeal cancer progression was promoted by a positive feedforward loop between *Fusobacterium nucleatum* and reprogramming of ethanol metabolism.[30] Together, this suggests a broader role of ethanol in alcohol-related cancers.

To acquire a better and more comprehensive view, a detailed characterization of the molecular effects of ethanol on human cells is needed. Here, we specifically study the response to ethanol using a non-cancerous, immortalized laryngeal cell line (HuLa-PC), to mimic the responses to ethanol in healthy epithelial tissue as closely as possible. To our knowledge, this represents the first detailed molecular study of the effects of ethanol on a healthy head and neck cell line.[23,24,28,31,32] Moreover, previous studies mostly focused on low ethanol concentrations that mirror typical blood concentrations. This prevents us from drawing a detailed picture of the responses to ethanol in healthy epithelial tissues, which often come into direct contact with the consumed alcohol and hence are exposed to levels that are much higher than blood alcohol levels.

Here, we use RNA sequencing to compare the effects of short-term and long-term ethanol exposure in HuLa-PC cells and identified the upregulation of genes involved in e.g., cytoskeleton remodeling and membrane ion transport, respectively. Furthermore, we find that ethanol slows down proliferation as well as replication fork progression. These effects were also observed in two head and neck cancer cell lines and two esophageal keratinocyte cell lines. Taken together, our data yields a comprehensive view of ethanol-stress responses in epithelial cells of the upper aerodigestive tract, which are a model for cells that come into direct contact with alcoholic beverages *in vivo*.

RESULTS

Ethanol affects cell survival in a dose- and time-dependent manner

To establish which concentrations of ethanol were tolerated by HuLa-PC cells *in vitro*, we assessed cell survival in different conditions. When people consume alcoholic beverages, the epithelial lining of the oral cavity and esophagus comes into direct contact with the beverage and its ethanol content. While typical blood alcohol concentrations after drinking range between 0 and 85 mM (0.50% v/v), which is life-threatening, epithelial cells can be exposed to much higher levels. Since the exact concentration to which epithelial cells are exposed depends on various factors, including the nature of the alcoholic beverage, dilution with saliva, and shielding by mucus layers, we chose to assess cell survival in a wide range of ethanol concentrations from 0 to 1000 mM (0%–5.84% v/v). As expected, the effect of ethanol on cell survival was dose- and time-dependent (Figure 1). When HuLa-PC cells were exposed for 4 h, only the highest ethanol concentration (1000 mM) induced a relatively minor decline in cell survival, i.e., 85% relative survival compared to the control. However, when HuLa-PC cells were exposed to ethanol for a prolonged time, even lower concentrations significantly decreased cell survival. The half maximal inhibitory concentration (IC50) was 425 and 375 mM ethanol at 24 h and 48 h exposure, respectively, as estimated by a fitted log dose-response curve (Figure S1A). We also assessed cell survival in response to ethanol in four other cell lines including two head and neck cancer cell lines, CAL-27 and SCC-61, and two immortalized esophageal keratinocyte cell lines, EPC1-hTERT and EPC2-hTERT. We observed a cell-line-dependent effect of ethanol as other cell lines showed different ethanol sensitivities (Figure S1). In line with our results for HuLa-PC cells, we find a dose- and time-dependent effect on survival for all the cell lines.

For subsequent experiments in HuLa-PC cells, we focused on 0–400 mM (2.34% v/v) or 0–250 mM (1.46% v/v) ethanol for short- and long-term experiments, respectively, since these were the treatment conditions that resulted in a relative survival above 75%.

Short- and long-term ethanol exposure differentially affects gene expression in HuLa-PC cells

To gain more insight into molecular pathways affected by ethanol, we used RNA sequencing to monitor the cells' transcriptional response to ethanol stress. Two different ethanol concentrations were used: 20 mM (0.12% v/v), a relevant blood alcohol concentration observed after

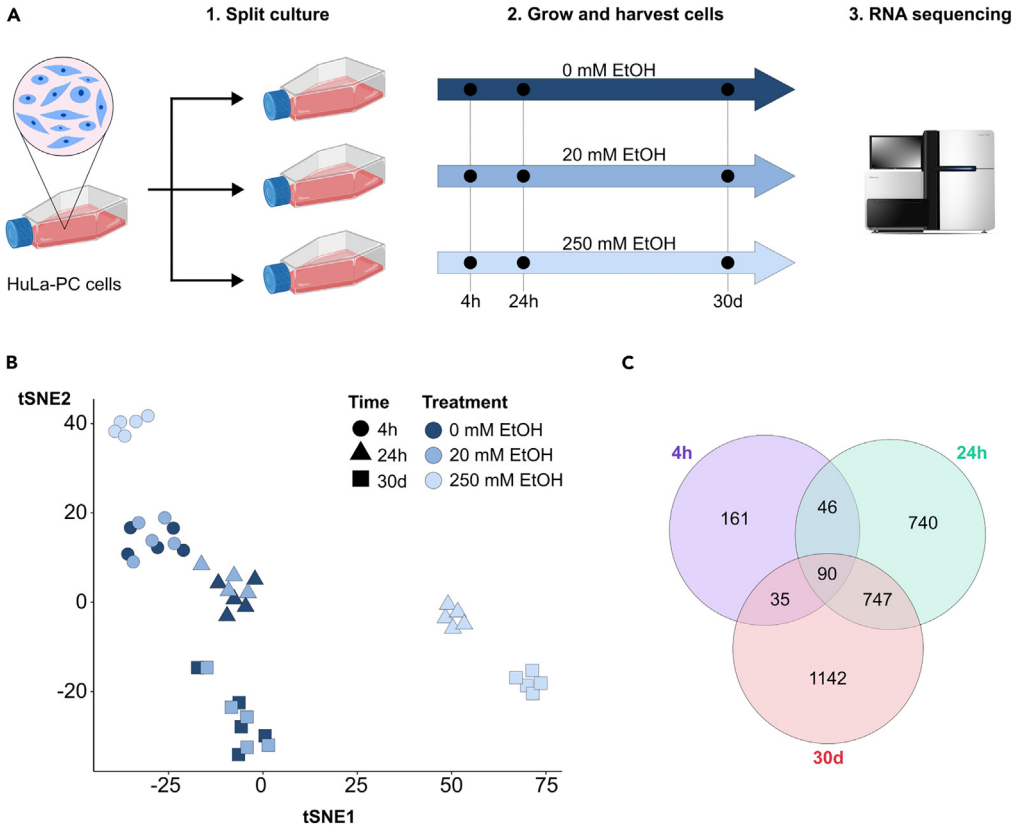

Figure 2. Bulk RNA sequencing of HuLa-PC cells exposed to ethanol shows that only 250 mM treatment results in differential gene expression patterns

(A) Set-up of the bulk RNA sequencing. One flask with HuLa-PC cells was split into three different subcultures at the start of the experiment. These subcultures were continuously grown in medium with 0, 20, or 250 mM ethanol (EtOH). Cells were harvested and RNA was extracted at 4 h (4 h), 24 h (24 h), and 30 days (30days). In total, five independent start cultures were treated, leading to a total of 5 independent biological replicates. Rendering of flasks was created with BioRender.com.

(B) t-SNE analysis of bulk RNA sequencing data was performed using the variance stabilized counts of the entire transcriptome (18,073 genes). Every symbol corresponds to an individual biological replicate. Note: one replicate of cells exposed to 20 mM ethanol for 24 h was excluded from this analysis because almost all gene counts were equal to zero.

(C) Venn diagram of differentially expressed genes in HuLa-PC cells treated with 250 mM ethanol. Genes with an absolute fold change larger than 2 and an adjusted p value smaller than 0.05 were considered differentially expressed.

"social drinking,"[33] and 250 mM (1.46% v/v), the highest concentration with minor effects on cell survival based on our previous data (Figure 1). Hula-PC cells were exposed to ethanol for 4 h, 24 h, or 30 days (Figure 2A). We included long-term ethanol exposure of 30 days to investigate whether cells could become ethanol tolerant or obtain more cancer-like properties after prolonged ethanol exposure. To minimize ethanol evaporation during incubation, flasks were placed in a "compensation system," as previously described.[34] We confirmed this system maintained the ethanol concentrations in our medium relatively stable and did not alter cell proliferation (Figure S2).

RNA sequencing data were mapped to the human reference genome GrCH38 by using the Spliced Transcripts Alignment to a Reference (STAR) algorithm[35] and a count matrix was generated with HTSeq.[36] Lowly expressed genes were removed from the gene count matrix, ultimately resulting in a transcriptome of 18,073 genes in HuLa-PC cells. A t-distributed Stochastic Neighbor Embedding (t-SNE) analysis[37] showed that the five biological replicates of each condition clustered together, demonstrating the reproducibility of our results (Figure 2B). Surprisingly, it also showed that the 20 mM ethanol-treated samples completely overlapped with the 0 mM ethanol-treated samples, indicating that there was no change in gene expression. We next used DESEq2[38] to analyze differential gene expression in ethanol-treated conditions relative to their respective controls. Genes with an absolute fold change larger than 2 and a Benjamini-Hochberg adjusted p value smaller than 0.05 were considered differentially expressed. This analysis indeed showed that exposure of HuLa-PC cells to 20 mM ethanol did not induce any significant changes in gene expression in any of the conditions. In contrast, we detected 332, 1623, and 2014 differentially expressed genes in HuLa-PC cells exposed to 250 mM ethanol for 4 h, 24 h, and 30 days, respectively (Figures 2C and S3).

Because only the exposure to 250 mM ethanol yielded significant differences in gene expression, we focused our further analyses on this condition. Gene Set Enrichment Analysis (GSEA)[39] was performed to gain more insight into biological processes that are activated or suppressed in ethanol stress. We compiled three ranked gene lists from the three exposure times to use as input for GSEA.[40] The ranking

was based on log2 fold changes, which were the output of DESEq2. We assessed the enrichment of gene ontology (GO) classification terms regarding biological process, molecular function, and cellular location. Because of redundancy, we focused on biological processes for visualization but the results of molecular function and cellular location enrichment are present in the source data file. Because many enriched biological process GOs were highly correlated, we clustered the top 30 most significant biological processes into functional groups based on pairwise similarities using the Jaccard's similarity index[41] (Figures 3, 4, and S4–S7). Overall, we observed similar families of downregulated biological processes when comparing the three ethanol exposure times. Genes belonging to GO terms related to transcription, translation, RNA transport, RNA processing, and ribosome biogenesis were significantly downregulated in ethanol-treated cells. For upregulated biological processes, there were some differences between the three time points. At 4 h of ethanol exposure, genes associated with cellular apoptosis and cytoskeleton organization were upregulated. At 24 h of ethanol exposure, genes linked to mesonephric development, inner ear development, response to nutrient levels, muscle contraction, and sodium ion transmembrane transport were upregulated. Lastly, 30 days of ethanol exposure resulted in the upregulation of genes related to kidney development, muscle contraction, water homeostasis, and sodium ion transmembrane transport.

Surprisingly, many of the upregulated genes show a link to organ development, e.g., kidney and ear development. We explored these gene lists in more detail and noticed multiple of these genes are signaling ligands, transmembrane receptors, and transcription factors. More specifically, various proteins of the Wnt signaling pathway were upregulated in ethanol-treated cells, including Wnt ligands and Frizzled class receptors (Figure S8A). Another signaling pathway that was activated in our ethanol-treated cells was interferon-γ signaling (Figures 4A and S8B). Interferon-γ is a known pro-inflammatory cytokine that is particularly important in immunomodulation.[42]

We also assessed the phenotype of HuLa-PC cells after long-term growth in ethanol-containing medium. We did not observe changes in population doubling time in growth medium with or without ethanol (Figure S9). These data suggest that 30 days of ethanol exposure did not induce ethanol tolerance or a more cancer-like phenotype in HuLa-PC cells.

In summary, our bulk RNA sequencing showed that ethanol stress decreased protein synthesis and gene expression in HuLa-PC cells, which was consistent across different exposure times. Upregulated genes were found to be associated with cytoskeleton organization and apoptosis, for short exposure times, or ion transport and muscle contraction, for longer exposure times. Together, ethanol exposure had a broad effect on the transcriptome by altering metabolic processes as well as developmental processes.

Ethanol slows down cell cycle and replication fork progression

Our RNA sequencing data indicated that ethanol-stressed cells vastly downregulated multiple processes important for basal protein synthesis such as ribosome biogenesis and translation. Downregulation of global protein synthesis is a hallmark of the integrated stress response, which can be triggered by multiple internal or external stress stimuli.[43] Since the G1 phase is generally characterized as the main growth phase,[44] we checked whether ethanol affects this particular cell cycle phase. We noticed that cyclin D-CDK4/6 complex proteins, which drive G1 to S phase progression,[45] were less abundant and several inhibitors of G1 cyclin-CDK complexes were overexpressed, indicating a suppression of G1 to S phase transition (Figure 5A). Cell cycle progression analysis of ethanol-exposed HuLa-PC cells indeed confirmed a G1 cell cycle phase delay with significantly more cells in the G1 phase between 24 h and 48 h of growth in ethanol-containing medium. (Figure 5B). Moreover, we confirmed an ethanol-induced G1 cell cycle phase delay both in head and neck cancer cells and esophageal keratinocytes (Figure S10). In cancer cells, the G1 delay was even still significant after 72 h of growth in ethanol (Figure S10). Next, we quantified the population doubling time of ethanol-treated cells and detected that these cells proliferated significantly slower. The doubling time increased 2-fold from 32 h to 64 h in medium that contained 250 mM ethanol (Figure 5C). This result was in agreement with the delayed cell cycle phase progression.

G1 cell-cycle arrest can be triggered by ribonucleotide depletion, which can activate p53 and p21, i.e., *CDKN1A*, in the absence of DNA damage.[46] Activation of p53 and p21 can not only trigger cell-cycle arrest, but these proteins are also regulators of replication fork progression.[47,48] Stalled replication forks or aberrant acceleration of fork progression fuel genomic instability, a hallmark of cancer.[49–51] Therefore, we investigated whether ethanol affected replication fork progression by using a DNA fiber analysis (Figure 5D). As a positive control, cells were exposed to methyl methane sulfonate (MMS), an alkylating drug known to stall replication forks.[52] Interestingly, ethanol significantly slowed down replication fork progression in HuLa-PC cells, albeit in a dose-dependent way (Figure 5E). Compared to non-treated control, HuLa-PC cells treated with 3 mM MMS or 400 mM EtOH showed an average delay in fork progression by 2.03 or 1.15 times respectively (Figure 5E). Noteworthy, 250 mM ethanol did have an effect, but this might be due to the short exposure time. We observed similar effects of ethanol on replication fork progression in our head and neck cancer cell lines and immortalized esophageal keratinocytes (Figure S11). The observed dose dependency in these different cell lines corresponded well with their ethanol sensitivity (Figure S1). We also assessed whether the aberrant replication fork progression resulted in the formation of double-strand DNA breaks (DSB), which can occur after fork collapse,[53] but we did not observe any significant induction of DSBs in ethanol-treated cells (Figure S12A). Similarly, head and neck cancer cells also showed no signs of DSBs when treated with ethanol (Figures S12B and S12C).

Collectively, Hula-PC cells exposed to ethanol proliferated significantly slower which might be linked to the altered cell cycle and replication fork progression. These results were consistent for five different cell lines, including two cancer cell lines.

Transient knockdown of acetaldehyde-producing genes does not alter the effects of ethanol in HuLa-PC cells

As indicated before, the carcinogenic effect of ethanol has mostly been attributed to its metabolites, i.e., ROS and acetaldehyde. We assessed whether ethanol exposure increased intracellular ROS in HuLa-PC cells, but we did not observe a significant induction (Figure S13). Therefore, we focused on investigating whether acetaldehyde is an important contributor to the biological effects of ethanol in HuLa-PC cells.

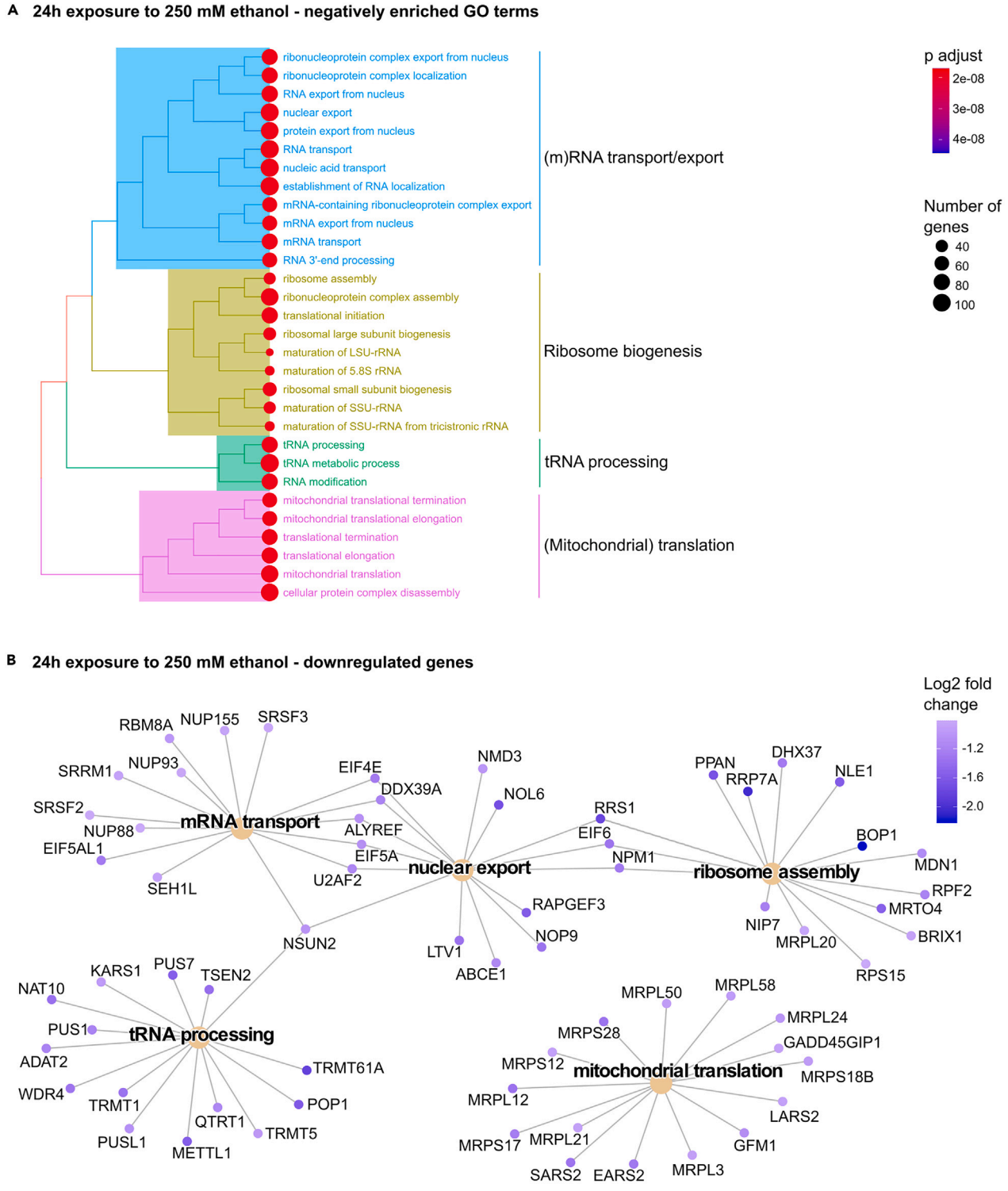

Figure 3. Treeplots and gene-concept networks of negatively enriched GO terms in HuLa-PC cells exposed for 24 h to 250 mM ethanol

(A) Treeplot of the top 30 most significant negatively enriched GO terms, corresponding to biological processes that are suppressed in ethanol-treated cells, as determined by GSEA. The color of the circles corresponds to the adjusted p value and the size of the circles represents the number of genes associated with that specific GO term. GO terms were clustered into categories by average linkage based on pairwise similarities using Jaccard's similarity index.

(B) Gene-concept network of a selection of suppressed biological processes. For each selected GO term, the top 15 most downregulated genes are visualized. The color of the nodes corresponds to the expression changes represented as log2 fold change.

A **24h exposure to 250 mM ethanol - positively enriched GO terms**

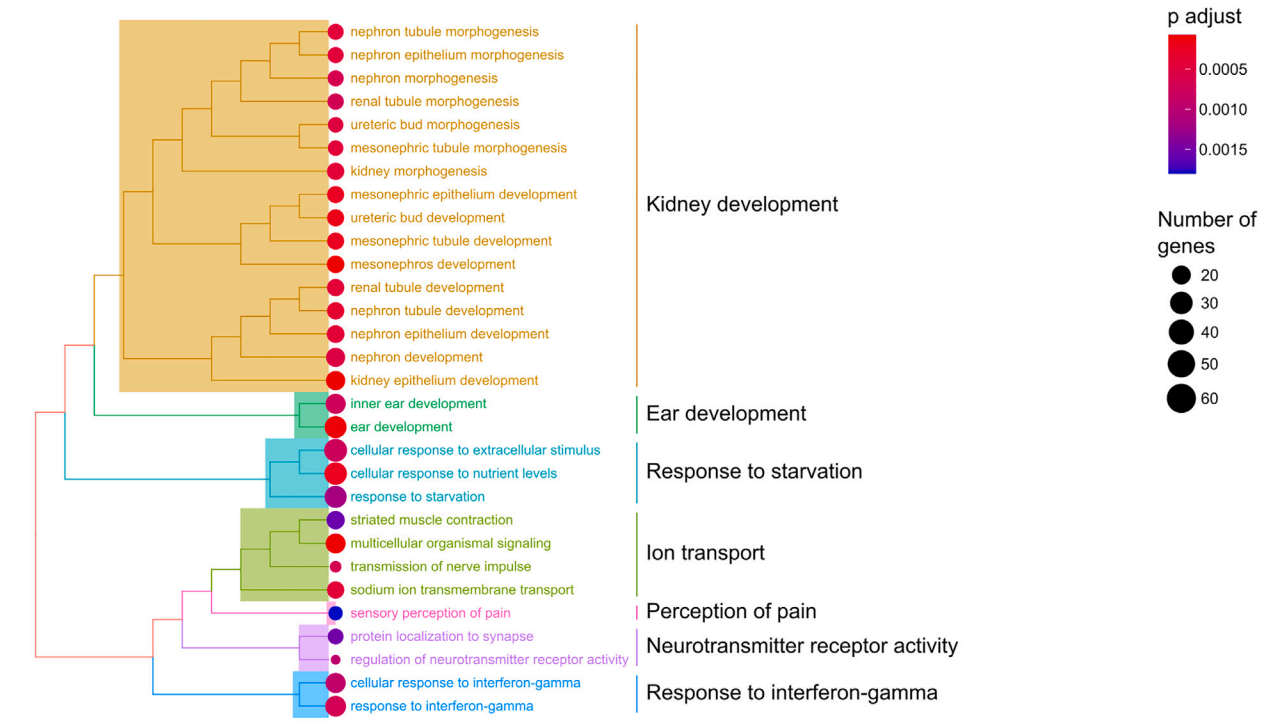

B **24h exposure to 250 mM ethanol - upregulated genes**

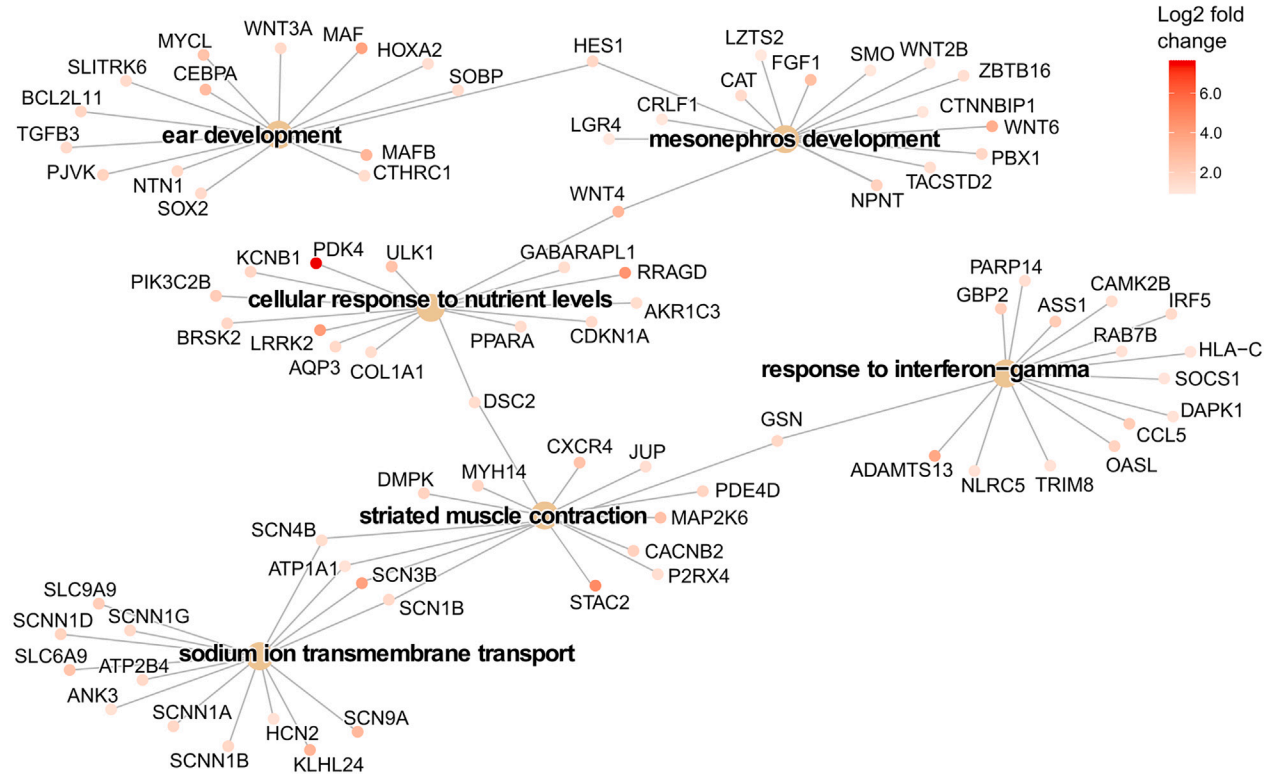

Figure 4. Treeplots and gene-concept networks of positively enriched GO terms in HuLa-PC cells exposed for 24 h to 250 mM ethanol

(A) Treeplot of the top 30 most significant positively enriched GO terms, corresponding to biological processes that are activated in ethanol-treated cells, as determined by GSEA. The color of the circles corresponds to the adjusted p value and the size of the circles represents the number of genes associated with that specific GO term. GO terms were clustered into categories by average linkage based on pairwise similarities using Jaccard's similarity index.

(B) Gene-concept network of a selection of activated biological processes. For each selected GO term, the top 15 most upregulated genes are visualized. The color of the nodes corresponds to the expression changes represented as log2 fold change.

Several gene products can oxidize ethanol into acetaldehyde, including multiple alcohol dehydrogenases (ADHs), cytochrome P450 enzymes, and catalase (CAT).[10] Based on our transcriptomics data, we focused on two genes, *ADH7* and *CAT*, that showed overexpression with a log2 fold change of 1.72 and 1.29, respectively at 30 days of exposure. Other ADHs known to oxidize ethanol were not expressed in our cell line. To minimize the formation of acetaldehyde in HuLa-PC cells, we transiently knocked down *ADH7* and *CAT* by targeted siRNAs. Targeted siRNAs reduced the RNA and protein levels of *ADH7* by 85% and 75%, respectively, relative to the not-transfected control. For *CAT*, a reduction of 87% and 67% was obtained on the RNA and protein levels, respectively, relative to the not-transfected control (Figures 6A, 6B, and 6C). We subsequently analyzed ethanol-induced changes in relative survival and replication fork progression as before in these knockdown cell lines. We found that cells with a targeted knockdown of *ADH7* and *CAT* behaved similarly to cells without this knockdown. Ethanol induced similar reductions in survival or replication fork progression in HuLa-PC cells transfected with targeted or non-targeted (NT) siRNAs (Figures 6D and 6E).

Taken together, these data suggest that the observed biological effects in HuLa-PC cells were directly linked to ethanol and not to intracellular ROS or acetaldehyde.

Ethanol exposure changes the cellular morphology of HuLa-PC cells

In our GSEA analysis, we observed that genes associated with cytoskeleton remodeling were activated after 4 h of ethanol exposure (Figure S5). Additionally, our RNA sequencing revealed a strong overexpression of multiple membrane-associated ion transporters that are involved in sodium ion homeostasis, muscle contraction, or membrane depolarization (Figure 7A). This might indicate that ethanol treatment induced membrane damage and leakage, which impaired cellular ion balances. We also noticed that ethanol exposure resulted in aberrant cell morphology compared to the cells in regular growth medium (Figure 7B). We quantified the cell area (in pixels), representing the cell size, and the aspect ratio, representing the cell's roundness. Clearly, ethanol-stressed cells were significantly smaller and rounder compared to control cells (Figures 7C and 7D).

Altogether, ethanol treatment resulted in the overexpression of multiple ion transporters and altered cell morphology which can both be linked to membrane stress.

DISCUSSION

Although ethanol is known to be toxic to all lifeforms and has been linked to multiple types of cancer, the underlying physiological and molecular effects on cells are still under investigation. We studied cellular stress responses to relatively high concentrations to obtain more insight into the molecular mechanisms affected by ethanol in tissues that come into direct contact with alcoholic beverages. Our data show that short- and long-term ethanol exposure affected gene expression patterns in HuLa-PC cells. Moreover, ethanol slowed down cell proliferation and replication fork progression in multiple epithelial cell lines of the upper aerodigestive tract.

We find striking similarities between our current work and our previous in-depth study in the model eukaryote *Saccharomyces cerevisiae*, including a slower cell cycle progression and replication fork stalling in ethanol-exposed cells.[21] Especially replication fork stalling is known to result in genomic instability, which could contribute to the development of malignancies.[49–51] To our knowledge, this is the first study showing that acute ethanol exposure has a direct effect on replication fork progression in human cells. We show that a 30-min exposure of HuLa-PC cells to 400 mM (2.34% v/v) ethanol significantly slowed down replication fork progression. Previously, it was reported that acetaldehyde treatment delays S-phase progression and induces replication stress in Chinese Hamster Ovarian cells and human esophageal keratinocytes.[54,55] These studies also reported extensive DNA damage in cells treated with acetaldehyde. Indeed, it has been described that acetaldehyde can induce interstrand DNA crosslinks which in turn can slow down replication fork progression.[56,57] However, acetaldehyde concentrations used in these previous studies[54,55] were around 1 mM, which is higher than the average salivary acetaldehyde concentrations of 50–150 μM after moderate alcohol consumption.[58,59] Hence, it is still unclear if physiologically relevant levels of acetaldehyde would result in similar phenotypes. Importantly, our results in transient knockdown cells indicate that ethanol-induced replication fork stalling did not depend on acetaldehyde production. Oxidative stress can also trigger replication fork stalling,[60] but we did not observe an induction of ROS in our ethanol-treated cells. Therefore, our current hypothesis for replication fork stalling is the stress-induced activation of cell cycle checkpoint regulators such as p53 and p21. P53 is the main transcriptional regulator of p21 that, in turn, can induce a G1 arrest and can negatively regulate replication fork speed.[49,61]

We also assessed the functional effects of ethanol in two HPV-negative head and neck cancer cell lines to investigate whether their responses differ from healthy epithelial cells. *TP53* is frequently inactivated in HPV-negative head and neck tumors.[62] Together with a loss of function of p16/CDKN2A and upregulation of cyclin D1, this often results in a dysfunctional G1/S checkpoint regulation.[63] However, we did observe a delay in G1 cell cycle progression in ethanol-treated cancer cells, which is consistent with our findings in healthy cells. Both CAL-27 and SCC-61 were shown to overexpress a mutated *TP53*,[64] which may indicate that p53 can still be active in these cell lines and

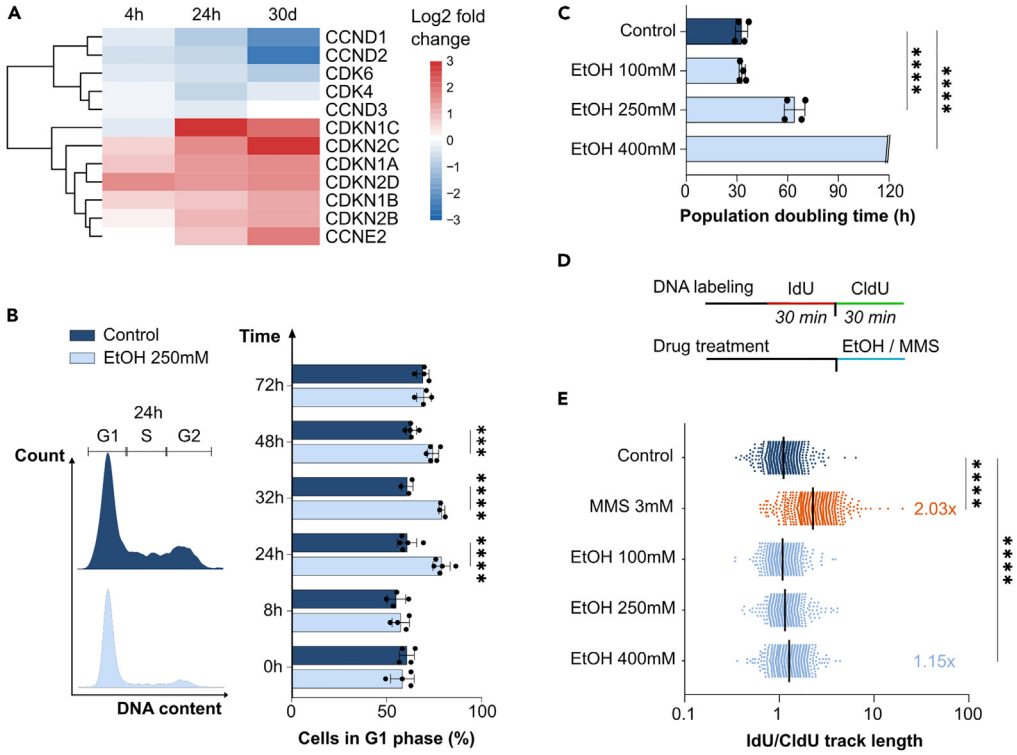

Figure 5. HuLa-PC cells show a G1 phase delay and a slower replication fork progression when exposed to ethanol

(A) Heatmap with expression changes of genes involved in G1 to S cell cycle phase transition in 250 mM ethanol-treated HuLa-PC cells. Expression changes are represented as log2 fold changes relative to the control cells, treated with 0 mM ethanol. Hierarchical clustering was performed by average linkage.

(B) Effect of ethanol (EtOH) on cell cycle distribution in Hula-PC cells. Two cell cycle profiles obtained after 24 h of ethanol exposure are depicted as an example. The graph indicates the percentage of cells in the G1 cell cycle phase in medium with or without ethanol. At least three individual biological replicates were measured, the bar indicates the average with standard deviation. Significance was assessed by a two-way ANOVA and a Šidák posthoc test to the respective control at the same time point. *** p-values <0.001, ****p < 0.0001.

(C) Effect of ethanol (EtOH) on population doubling time in HuLa-PC cells. Four independent biological replicates were measured, the bar indicates the average with standard deviation. At 400 mM ethanol, no growth was observed which is indicated by a capped bar. Statistical significance was determined by a one-way ANOVA with a Dunnett posthoc test. ****p < 0.0001.

(D) DNA labeling scheme for the DNA fiber analysis. Cells were consecutively treated with 5-iodo-2′-deoxyuridine (IdU) and 5-chloro-2′-deoxyuridine (CldU). Both pulses were exactly 30 min and ethanol (EtOH) or MMS was added during the second pulse only.

(E) Effect of ethanol (EtOH) or MMS on replication fork progression in HuLa-PC cells assessed by a DNA fiber analysis. Cells were labeled and treated as specified in panel (D). The ratio of IdU/CldU track length is depicted. For each condition, four independent biological replicates were assessed, with a minimum of 150 fibers each. Each dot corresponds to a measurement of an individual DNA fiber, the black bar represents the average IdU/CldU ratio. The fold change with respect to the control is also indicated on the graph. Number of scored fibers: Control = 990; MMS = 520; EtOH 100 mM = 549; EtOH 250 mM = 607; EtOH 400 mM = 616. Statistical significance was assessed by a Welch-corrected one-way ANOVA with Games-Howell posthoc test on log-transformed ratios. ****p < 0.0001.

regulate the G1/S checkpoint. Similar to healthy cells, we observed replication fork stalling in ethanol-treated cancer cells which did not result in the induction of double-strand DNA breaks. Together, our results seem to indicate a similar mode of action of ethanol in both cancer and non-cancer epithelial cells.

Our RNA sequencing data indicated that 20 mM ethanol did not induce differential gene expression in HuLa-PC cells, which corroborates previous findings in esophageal keratinocytes where 17 mM (0.1% v/v) ethanol treatment did not alter gene expression patterns.[24] Contrarily, we observed altered gene expression patterns in cells treated with 250 mM ethanol. Similarly as in,[24] our results indicated that ethanol induced mitochondrial stress, as GO terms "mitochondrial ATP synthesis coupled electron transport," "mitochondrial respiratory chain complex assembly," and "mitochondrial gene expression" were negatively enriched in our GSEA results. Surprisingly, we detected no clear induction of proteotoxic stress or oxidative stress responses in HuLa-PC, which is in contrast to previous studies.[23–25,65] Noteworthy, the control samples in Figure 2B are not clustering together suggesting that not only ethanol exposure but also the propagation time of HuLa-PC cells *in vitro* induced gene expression alterations. This was not unexpected as it has been shown before that long-term culturing of cells *in vitro* induces changes in global expression patterns.[66,67] Our data indicated that HuLa-PC cells did not exhibit any phenotypic differences after 30 days of growth in 250 mM ethanol-containing medium. This is in contrast to results obtained in human

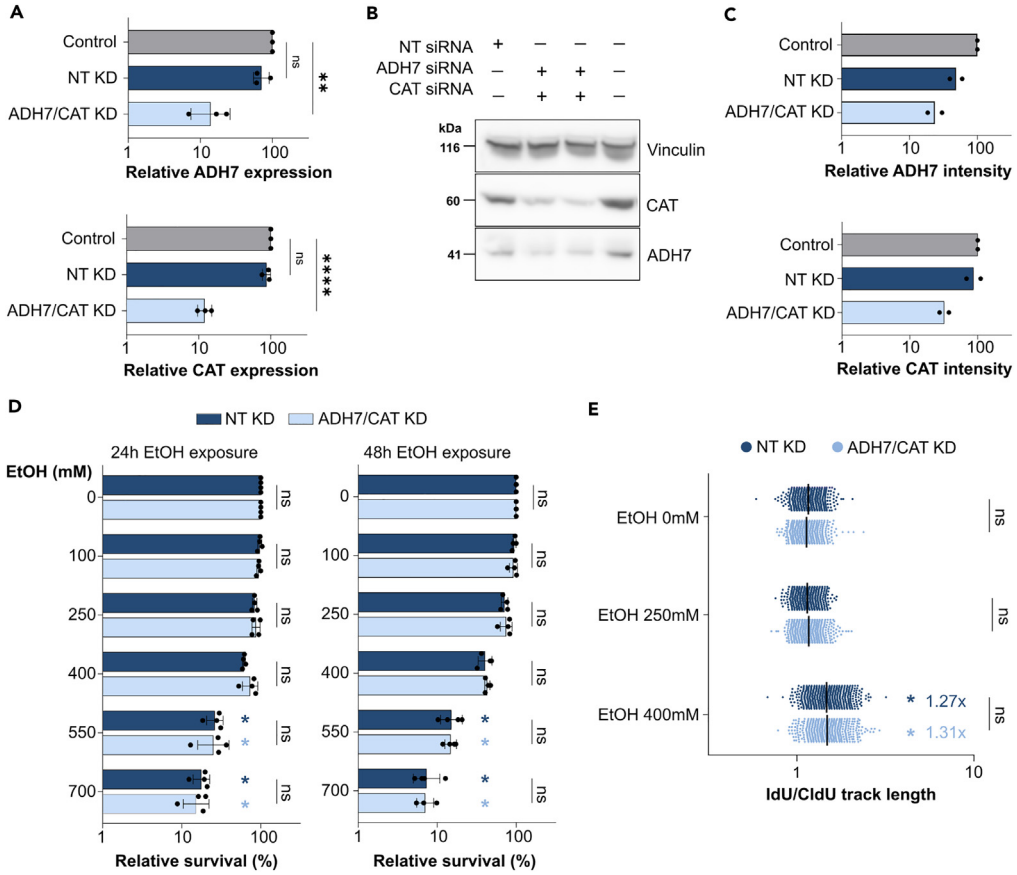

Figure 6. Targeted knockdown of ethanol-metabolizing genes does not alter the effects of ethanol in HuLa-PC cells

(A) Gene knockdown of the ADH7 and CAT genes was assessed on the RNA level, with qRT-PCR, 24 h after transfection. Quantification of relative expression, as calculated by the ΔΔCt method54, is depicted. "Control" corresponds to not-transfected cells, "NT KD" is non-targeted control knockdown, and "ADH7/CAT KD" is a targeted knockdown of both ADH7 and CAT. Three biological replicates were assessed and the bar represents the average with standard deviation. Significance was assessed by a one-way ANOVA with a Dunnett posthoc test on log-transformed values. **$p < 0.01$, ****$p < 0.0001$.

(B Immunoblots of transfected cells to check knockdown on the protein level 24 h after transfection. The full uncropped Western blot is visualized in Figure S14.

(C) Relative protein band signals as quantified by densitometry. Two individual replicates were quantified.

(D) Effect of ethanol (EtOH) on relative survival in transfected HuLa-PC cells. "NT KD" is non-targeted control knockdown, and "ADH7/CAT KD" is a targeted knockdown of both ADH7 and CAT. At least three independent replicates were analyzed and the bar represents the average with standard deviation. Statistical significance was assessed by a two-way ANOVA with a Šidák posthoc test on log-transformed relative survival data. Dark and light blue asterisks indicate a significant reduction in survival due to ethanol exposure. *$p < 0.05$. The specific siRNA knockdown had no significant effect on survival in ethanol as indicated by not significant (ns).

(E) Effect of ethanol (EtOH) on replication fork progression in transfected HuLa-PC cells. "NT KD" is non-targeted control knockdown, and "ADH7/CAT KD" is a targeted knockdown of both ADH7 and CAT. The DNA labeling was identical as in Figure 4D. Four independent biological replicates were assessed, with minimally 100 fibers each. Each dot corresponds to a measurement of an individual DNA fiber, the black bar represents the average IdU/CldU ratio. The fold change with respect to the 0 mM treated cells is also indicated in the graph. Number of scored DNA fibers: NT 0 mM EtOH = 605; NT 250 mM EtOH = 582; NT 400 mM EtOH = 593; ADH7/CAT KD 0 mM EtOH = 582; ADH7/CAT KD 250 mM EtOH = 601; ADH7/CAT KD 400 mM EtOH = 510. Statistical significance was assessed by a Welch-corrected ANOVA with Games-Howell posthoc test on log-transformed ratios. *$p < 0.05$.

pancreatic normal ductal epithelial cells,[68] but the discrepancy may be explained by the difference in ethanol exposure time, i.e., 6 months[68] versus 30 days.

However, several highly upregulated genes in ethanol-exposed cells show a link to tumor formation. Firstly, multiple Wnt signaling ligands and receptors were overexpressed in our ethanol-exposed cells. Upregulation of Wnt signaling was also observed in colon organoids treated with 35 mM (0.20% v/v) ethanol for 72 h.[23] In addition, upregulation of the non-canonical Wnt signaling pathway was observed in cardiomyocytes treated with 50 mM (0.29% v/v) ethanol for 5 weeks.[69] Wnt signaling has been shown to promote epithelial to mesenchymal transition which in turn can promote cell migration and tumor metastasis.[28,70,71] For instance, *WNT4* was overexpressed in colon cancer tissues and treatment of colon cancer cells with Wnt4 increased cell invasion and migration *in vitro*.[72] In our HuLa-PC cells, we saw a strong induction of *WNT4* as well with a fold change of 8.11 and 2.74 at 24 h and 30 days exposure respectively. Additionally, the Jun

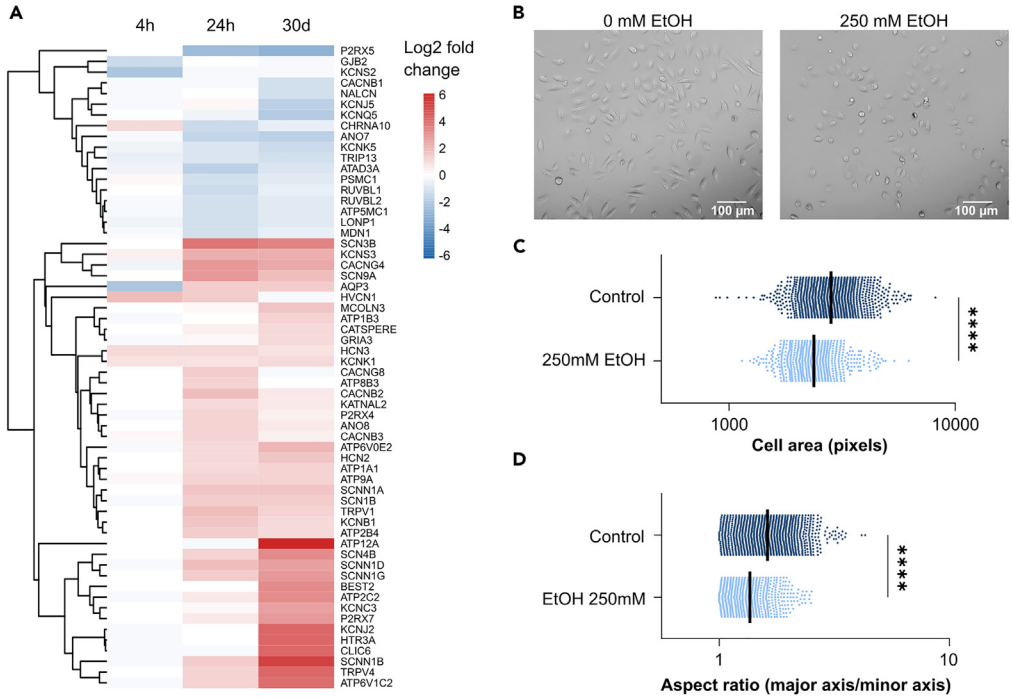

Figure 7. HuLa-PC cells upregulate membrane-associated ion transporters and show a different morphology when grown in ethanol-containing medium

(A) Heatmap of genes involved in ion transport. All ion transporters with an absolute fold change larger than 2 and an adjusted p value smaller than 0.05 in minimally one condition were selected. Expression changes are represented as log2 fold changes relative to the control cells, treated with 0 mM ethanol. Hierarchical clustering was performed by average linkage.

(B) Effect of ethanol (EtOH) on cell morphology in HuLa-PC cells. Representative bright field pictures showing the morphology of cells grown in normal growth medium or ethanol-containing medium during 48 h.

(C and D) Quantification of the pixel area and the aspect ratio was performed in ImageJ. Imaging was performed on three individual biological replicates, each consisting of a minimum of 200 cells. Each dot corresponds to a measurement of an individual cell. The black line indicates the mean. Statistical significance was assessed by a two-tailed Mann-Whitney test. ****$p < 0.0001$. Number of scored cells: Control = 1160, 250 mM EtOH = 615.

transcription factor is involved to activate target genes of the non-canonical Wnt signaling pathway. We observed the upregulation of *JUNB*, *JUN*, and *JUND* in our ethanol-treated cells. *JUNB* is a proto-oncogene and increases the cell metastasis potential of head and neck cancer cell lines.[73] Taken together, this could indicate that exposing cells to ethanol can cause cells to acquire cancer-like properties, such as increased migration capacity, through Wnt signaling. Intriguingly, targeting the Wnt signaling pathway might also have therapeutic value, with recent studies showing that inhibiting Wnt signaling can be a potential therapeutic route for head and neck cancers.[74,75] Lastly, we observed a strong up-regulation of the glycoprotein NMB (*GPNMB*) with a fold change of 2.7 and 11.5 at 24 h and 30 days ethanol stress respectively. Recent proteomics analysis showed that this protein was 50-fold more abundant in alcohol-associated hepatitis tissues.[76] Furthermore, *GPNMB* is overexpressed in oral, laryngeal, and head and neck squamous cell carcinoma and can promote malignant progression.[77,78] Therefore, *GPNBM* might be an interesting biomarker for alcohol consumption to investigate with regard to alcohol-associated diseases.

In addition, we compared our bulk RNA sequencing data to the data obtained in the study of Gao et al. (GSE142083) who performed a full transcriptome analysis of 53 primary laryngeal squamous cell carcinomas.[79] Comparing the expression profiles of patients with and without an alcohol history revealed some interesting overlaps with our results. In alcohol-related laryngeal tumor samples, biological processes such as ribosomal biogenesis, mitochondrial gene expression, and RNA transport are suppressed while interferon-gamma production and keratinization are activated. These trends are similar to our GSEA results, obtained from laryngeal epithelial cells exposed to ethanol *in vitro*.

Aside from functional and transcriptomic effects, ethanol-treated HuLa-PC cells showed an aberrant cell morphology. Our observations are in agreement with the results of Kar et al. who observed cell shrinkage and actin filament disorganization in ethanol-treated mouse fibroblasts.[80] Because we also noticed a strong upregulation of genes coding for membrane-associated ion transporters, we hypothesize that ethanol treatment results in membrane damage and leakage. Indeed, previous research indicated that ethanol affects cell membrane fluidity and increased permeability.[26,80,81] Similarly, ethanol is known to cause increased membrane permeability as well as changes in membrane composition in *S. cerevisiae*.[82,83] It is currently unclear if and how ethanol-associated membrane damage could initiate carcinogenesis. However, increased membrane permeability can increase exposure to other carcinogens, e.g., those coming from tobacco smoke, which can explain the strong synergy between alcohol and tobacco in oral cancer risk.[84–86]

In summary, we paint a detailed picture of ethanol stress responses in epithelial cells of the upper aerodigestive tract. Our results confirm that ethanol has pleiotropic effects on eukaryotic cells. Most strikingly, we find that acute ethanol exposure directly affects replication fork progression which could affect genome stability in cells. Additionally, we detect the upregulation of several genes that are linked to alcohol-associated diseases, which highlights the validity of our model. Together, these data form a stepping stone toward new paradigms in ethanol-related carcinogenesis.

Limitations of the study

Because most cited mechanisms in ethanol-related carcinogenesis are linked to acetaldehyde, we also tried to elucidate the importance of acetaldehyde in the effects of ethanol on cells. However, we did not quantify intracellular levels of acetaldehyde upon ethanol exposure and transient knockdown since acetaldehyde is extremely reactive and therefore very difficult to accurately quantify in cell lysates. Hence, we cannot draw definitive conclusions from our data. Furthermore, we used an *in vitro* cell model to characterize the molecular effects of ethanol exposure. These mono-cultures do not fully reflect the oral epithelium *in vivo* and its complex interplay between epithelial, immune cells and fibroblast. Therefore, future studies are needed to confirm if ethanol exposure affects the same pathways *in vivo*. Another drawback of *in vitro* studies is that they might not be completely representative of the real-life situation of drinking alcoholic beverages. However, we believe that for instance the acute ethanol exposure for 30 min, which we used to study replication stress, can mimic the act of drinking. Ethanol is a small amphiphilic molecule that readily diffuses through cellular membranes.[87] Hence, when people consume alcoholic beverages, the oral mucosa will be exposed to high ethanol concentrations for a short time. Additionally, the alcoholic content of beverages is usually much higher than the 400 mM (2.34% v/v) ethanol to which we exposed our cells.

STAR★METHODS

Detailed methods are provided in the online version of this paper and include the following:

- KEY RESOURCES TABLE
- RESOURCE AVAILABILITY
  - Lead contact
  - Materials availability
  - Data and code availability
- EXPERIMENTAL MODEL AND STUDY PARTICIPANT DETAILS
  - Cell lines and reagents
- METHOD DETAILS
  - Ethanol treatment
  - Cell survival and proliferation
  - Bulk RNA sequencing and analysis
  - Cell cycle analysis
  - DNA fiber analysis
  - Immunofluorescence to detect DNA damage
  - Quantification of intracellular reactive oxygen species
  - Transient gene knockdown
  - RNA isolation, cDNA synthesis, quantitative reverse-transcription polymerase chain reaction (qRT-PCR)
  - Immunoblotting
  - Analysis of cell morphology
- QUANTIFICATION AND STATISTICAL ANALYSIS

SUPPLEMENTAL INFORMATION

Supplemental information can be found online at https://doi.org/10.1016/j.isci.2023.108564.

ACKNOWLEDGMENTS

We want to thank Prof. M.D. Hiroshi Nakagawa (Herbert Irving Comprehensive Cancer Center, Columbia University, New York, USA) for kindly sharing the EPC1-hTERT and EPC2-hTERT cell lines with our laboratory, Prof. Peter Van Loo and Dr. Jonas Demeulemeester for productive discussions regarding sequencing data analysis. We also want to acknowledge the VIB Bio Imaging Core for their support and assistance with image acquisition performed for this article. This work was financially supported by a grant from Research Foundation Flanders (FWO) to S.N., K.V., and K.J.V. - grant number G090618N. L.H. was supported by a PhD fellowship from FWO (11B6720N). S.N. is supported by a clinical research mandate from the Flemish Foundation of Scientific Research (FWO-Vlaanderen, 18B4122N). R.D. is supported by the Emmanuel van der Schueren fellowship for postdoctoral researchers from Kom op tegen Kanker and the Flemish Foundation of Scientific Research (FWO-Vlaanderen, 1521019N).

AUTHOR CONTRIBUTIONS

Experimental work: L.H.; methodology and design of experiments: L.H., K.V., and R.D.; data-analysis: L.H., B.B., D.L., B.S., S.K.G., D.G., and P.P.; data visualization: L.H.; writing - original draft: L.H., K.V., and R.D.; writing - review & editing: L.H., K.V., R.D., K.J.V., S.N., S.K.G., B.S., D.L., B.B., P.P., and D.G.; supervision: K.J.V. and S.N.; funding acquisition: L.H., K.V., K.J.V., and S.N.

DECLARATION OF INTERESTS

The authors declare no conflict of interest.

Received: July 13, 2023
Revised: October 11, 2023
Accepted: November 21, 2023
Published: November 23, 2023

REFERENCES

1. World Health Organization (2018). Global Status Report on Alcohol and Health 2018 (World Health Organization).
2. Rumgay, H., Shield, K., Charvat, H., Ferrari, P., Sornpaisarn, B., Obot, I., Islami, F., Lemmens, V.E.P.P., Rehm, J., and Soerjomataram, I. (2021). Global burden of cancer in 2020 attributable to alcohol consumption: a population-based study. Lancet Oncol. *22*, 1071–1080.
3. Baan, R., Straif, K., Grosse, Y., Secretan, B., El Ghissassi, F., Bouvard, V., Altieri, A., and Cogliano, V.; WHO International Agency for Research on Cancer Monograph Working Group (2007). Carcinogenicity of alcoholic beverages. Lancet Oncol. *8*, 292–293.
4. Seitz, H.K., and Stickel, F. (2007). Molecular mechanisms of alcohol-mediated carcinogenesis. Nat. Rev. Cancer *7*, 599–612.
5. Soffritti, M., Belpoggi, F., Cevolani, D., Guarino, M., Padovani, M., and Maltoni, C. (2002). Results of Long-Term Experimental Studies on the Carcinogenicity of Methyl Alcohol and Ethyl Alcohol in Rats. Ann. N. Y. Acad. Sci. *982*, 46–69.
6. IARC Working Group on the Evaluation of Carcinogenic Risks to Humans (2010). Alcohol consumption and ethyl carbamate. IARC Monogr. Eval. Carcinog. Risks Hum. *96*, 3–1383.
7. Gormley, M., Creaney, G., Schache, A., Ingarfield, K., and Conway, D.I. (2022). Reviewing the epidemiology of head and neck cancer: definitions, trends and risk factors. Br. Dent. J. *233*, 780–786.
8. Di Credico, G., Polesel, J., Dal Maso, L., Pauli, F., Torelli, N., Luce, D., Radoï, L., Matsuo, K., Serraino, D., Brennan, P., et al. (2020). Alcohol drinking and head and neck cancer risk: the joint effect of intensity and duration. Br. J. Cancer *123*, 1456–1463.
9. Zakhari, S. (2006). Overview: How is alcohol metabolized by the body? Alcohol Res. Health *29*, 245–254.
10. Hoes, L., Dok, R., Verstrepen, K.J., and Nuyts, S. (2021). Ethanol-Induced Cell Damage Can Result in the Development of Oral Tumors. Cancers *13*, 3846.
11. Garaycoechea, J.I., Crossan, G.P., Langevin, F., Mulderrig, L., Louzada, S., Yang, F., Guilbaud, G., Park, N., Roerink, S., Nik-Zainal, S., et al. (2018). Alcohol and endogenous aldehydes damage chromosomes and mutate stem cells. Nature *553*, 171–177.
12. Yokoyama, A., and Omori, T. (2003). Genetic Polymorphisms of Alcohol and Aldehyde Dehydrogenases and Risk for Esophageal and Head and Neck Cancers. Jpn. J. Clin. Oncol. *33*, 111–121.
13. Chang, J.S., Hsiao, J.R., and Chen, C.H. (2017). ALDH2 polymorphism and alcohol-related cancers in Asians: A public health perspective Tse-Hua Tan. J. Biomed. Sci. *24*, 1–10.
14. Chang, J., Tan, W., Ling, Z., Xi, R., Shao, M., Chen, M., Luo, Y., Zhao, Y., Liu, Y., Huang, X., et al. (2017). Genomic analysis of oesophageal squamous-cell carcinoma identifies alcohol drinking-related mutation signature and genomic alterations. Nat. Commun. *8*, 15290.
15. Ko, J.M.-Y., Guo, C., Liu, C., Ning, L., Dai, W., Tao, L., Lo, A.W.-I., Wong, C.W.-Y., Wong, I.Y.-H., Chan, F.S.-Y., et al. (2022). Clonal relationship and alcohol consumption-associated mutational signature in synchronous hypopharyngeal tumours and oesophageal squamous cell carcinoma. Br. J. Cancer *127*, 2166–2174.
16. Plath, M., Gass, J., Hlevnjak, M., Li, Q., Feng, B., Hostench, X.P., Bieg, M., Schroeder, L., Holzinger, D., Zapatka, M., et al. (2021). Unraveling most abundant mutational signatures in head and neck cancer. Int. J. Cancer *148*, 115–127.
17. Supek, F., and Lehner, B. (2017). Clustered Mutation Signatures Reveal that Error-Prone DNA Repair Targets Mutations to Active Genes. Cell *170*, 534–547.e23.
18. Wang, Y., Millonig, G., Nair, J., Patsenker, E., Stickel, F., Mueller, S., Bartsch, H., and Seitz, H.K. (2009). Ethanol-induced cytochrome P4502E1 causes carcinogenic etheno-DNA lesions in alcoholic liver disease. Hepatology *50*, 453–461.
19. Hirohashi, K., Ohashi, S., Amanuma, Y., Nakai, Y., Ida, T., Baba, K., Mitani, Y., Mizumoto, A., Yamamoto, Y., Kikuchi, O., et al. (2020). Protective effects of Alda-1, an ALDH2 activator, on alcohol-derived DNA damage in the esophagus of human ALDH2*2 (Glu504Lys) knock-in mice. Carcinogenesis *41*, 194–202.
20. Balbo, S., Juanes, R.C., Khariwala, S., Baker, E.J., Daunais, J.B., and Grant, K.A. (2016). Increased levels of the acetaldehyde-derived DNA adduct N2-ethyldeoxyguanosine in oral mucosa DNA from Rhesus monkeys exposed to alcohol. Mutagenesis *31*, 553–558.
21. Voordeckers, K., Colding, C., Grasso, L., Pardo, B., Hoes, L., Kominek, J., Gielens, K., Dekoster, K., Gordon, J., Van der Zande, E., et al. (2020). Ethanol exposure increases mutation rate through error-prone polymerases. Nat. Commun. *11*, 3664.
22. Liu, C., Marioni, R.E., Hedman, Å.K., Pfeiffer, L., Tsai, P.-C., Reynolds, L.M., Just, A.C., Duan, Q., Boer, C.G., Tanaka, T., et al. (2018). A DNA methylation biomarker of alcohol consumption. Mol. Psychiatry *23*, 422–433.
23. Devall, M., Plummer, S.J., Bryant, J., Jennelle, L.T., Eaton, S., Dampier, C.H., Huyghe, J.R., Peters, U., Powell, S.M., and Casey, G. (2021). Ethanol exposure drives colon location specific cell composition changes in a normal colon crypt 3D organoid model. Sci. Rep. *11*, 432.
24. Chandramouleeswaran, P.M., Guha, M., Shimonosono, M., Whelan, K.A., Maekawa, H., Sachdeva, U.M., Ruthel, G., Mukherjee, S., Engel, N., Gonzalez, M.V., et al. (2020). Autophagy mitigates ethanol-induced mitochondrial dysfunction and oxidative stress in esophageal keratinocytes. PLoS One *15*, e0239625.
25. Hernandez, C., Blanc, E.B., Pène, V., Le-Grand, B., Villaret, M., Aoudjehane, L., Carpentier, A., Conti, F., Calmus, Y., Podevin, P., et al. (2020). Impact of hepatitis C virus and alcohol, alone and combined, on the unfolded protein response in primary human hepatocytes. Biochimie *168*, 17–27.
26. Patra, M., Salonen, E., Terama, E., Vattulainen, I., Faller, R., Lee, B.W., Holopainen, J., and Karttunen, M. (2006). Under the influence of alcohol: The effect of ethanol and methanol on lipid bilayers. Biophys. J. *90*, 1121–1135.
27. Gelfand, R., Vernet, D., Bruhn, K., Vadgama, J., and Gonzalez-Cadavid, N.F. (2016). Long-term exposure of MCF-12A normal human breast epithelial cells to ethanol induces epithelial mesenchymal transition and oncogenic features. Int. J. Oncol. *48*, 2399–2414.
28. Chen, D., Yu, D., Wang, X., Liu, Y., He, Y., Deng, R., Jiang, Y., Zhang, F., Liu, Y., Xu, M., et al. (2018). Epithelial to mesenchymal transition is involved in ethanol promoted hepatocellular carcinoma cells metastasis and stemness. Mol. Carcinog. *57*, 1358–1370.
29. Zheng, K., Yu, J., Chen, Z., Zhou, R., Lin, C., Zhang, Y., Huang, Z., Yu, L., Zhao, L., and Wang, Q. (2019). Ethanol promotes

alcohol-related colorectal cancer metastasis via the TGF-β/RUNX3/Snail axis by inducing TGF-β1 upregulation and RUNX3 cytoplasmic mislocalization. EBioMedicine *50*, 224–237.
30. Hsueh, C.-Y., Huang, Q., Gong, H., Shen, Y., Sun, J., Lau, H.-C., Zhang, D., Tang, D., Wu, C., Guo, Y., et al. (2022). A positive feed-forward loop between Fusobacterium nucleatum and ethanol metabolism reprogramming drives laryngeal cancer progression and metastasis. iScience *25*, 103829.
31. Nguyen, A., Kim, A.H., Kang, M.K., Park, N.H., Kim, R.H., Kim, Y., and Shin, K.H. (2022). Chronic Alcohol Exposure Promotes Cancer Stemness and Glycolysis in Oral/Oropharyngeal Squamous Cell Carcinoma Cell Lines by Activating NFAT Signaling. Int. J. Mol. Sci. *23*, 9779.
32. Zhao, M., Howard, E.W., Guo, Z., Parris, A.B., and Yang, X. (2017). P53 pathway determines the cellular response to alcohol-induced DNA damage in MCF-7 breast cancer cells. PLoS One *12*, e0175121.
33. Abraham, J., Balbo, S., Crabb, D., and Brooks, P.J. (2011). Alcohol metabolism in human cells causes DNA damage and activates the Fanconi anemia – breast cancer susceptibility (FA-BRCA) DNA damage response network. Alcohol Clin. Exp. Res. *35*, 2113–2120.
34. Eysseric, H., Gonthier, B., Soubeyran, A., Bessard, G., Saxod, R., and Barret, L. (1997). There is no simple method to maintain a constant ethanol concentration in long-term cell culture: Keys to a solution applied to the survey of astrocytic ethanol absorption. Alcohol *14*, 111–115.
35. Dobin, A., Davis, C.A., Schlesinger, F., Drenkow, J., Zaleski, C., Jha, S., Batut, P., Chaisson, M., and Gingeras, T.R. (2013). STAR: ultrafast universal RNA-seq aligner. Bioinformatics *29*, 15–21.
36. Anders, S., Pyl, P.T., and Huber, W. (2015). HTSeq–a Python framework to work with high-throughput sequencing data. Bioinformatics *31*, 166–169.
37. Van der Maaten, L., and Hinton, G. (2008). Visualizing data using t-SNE. J. Mach. Learn. Res. *9*, 2579–2605.
38. Love, M.I., Huber, W., and Anders, S. (2014). Moderated estimation of fold change and dispersion for RNA-seq data with DESeq2. Genome Biol. *15*, 550.
39. Subramanian, A., Tamayo, P., Mootha, V.K., Mukherjee, S., Ebert, B.L., Gillette, M.A., Paulovich, A., Pomeroy, S.L., Golub, T.R., Lander, E.S., and Mesirov, J.P. (2005). Gene set enrichment analysis: A knowledge-based approach for interpreting genome-wide expression profiles. Proc. Natl. Acad. Sci. USA *102*, 15545–15550.
40. Reimand, J., Isserlin, R., Voisin, V., Kucera, M., Tannus-Lopes, C., Rostamianfar, A., Wadi, L., Meyer, M., Wong, J., Xu, C., et al. (2019). Pathway enrichment analysis and visualization of omics data using g:Profiler, GSEA, Cytoscape and EnrichmentMap. Nat. Protoc. *14*, 482–517.
41. Wu, T., Hu, E., Xu, S., Chen, M., Guo, P., Dai, Z., Feng, T., Zhou, L., Tang, W., Zhan, L., et al. (2021). clusterProfiler 4.0: A universal enrichment tool for interpreting omics data. Innov *2*, 100141.
42. Schroder, K., Hertzog, P.J., Ravasi, T., and Hume, D.A. (2004). Interferon-γ: an overview of signals, mechanisms and functions. J. Leukoc. Biol. *75*, 163–189.
43. Pakos-Zebrucka, K., Koryga, I., Mnich, K., Ljujic, M., Samali, A., and Gorman, A.M. (2016). The integrated stress response. EMBO Rep. *17*, 1374–1395.
44. Morgan, D.O. (2007). The Cell Cycle: Principles of Control (New science press).
45. Bertoli, C., Skotheim, J.M., and de Bruin, R.A.M. (2013). Control of cell cycle transcription during G1 and S phases. Nat. Rev. Mol. Cell Biol. *14*, 518–528.
46. Linke, S.P., Clarkin, K.C., Di Leonardo, A., Tsou, A., and Wahl, G.M. (1996). A reversible, p53-dependent G0/G1 cell cycle arrest induced by ribonucleotide depletion in the absence of detectable DNA damage. Genes Dev. *10*, 934–947.
47. Klusmann, I., Rodewald, S., Müller, L., Friedrich, M., Wienken, M., Li, Y., Schulz-Heddergott, R., and Dobbelstein, M. (2016). p53 Activity Results in DNA Replication Fork Processivity. Cell Rep. *17*, 1845–1857.
48. Galanos, P., Vougas, K., Walter, D., Polyzos, A., Maya-Mendoza, A., Haagensen, E.J., Kokkalis, A., Roumelioti, F.-M., Gagos, S., Tzetis, M., et al. (2016). Chronic p53-independent p21 expression causes genomic instability by deregulating replication licensing. Nat. Cell Biol. *18*, 777–789.
49. Maya-Mendoza, A., Moudry, P., Merchut-Maya, J.M., Lee, M., Strauss, R., and Bartek, J. (2018). High speed of fork progression induces DNA replication stress and genomic instability. Nature *559*, 279–284.
50. Gaillard, H., García-Muse, T., and Aguilera, A. (2015). Replication stress and cancer. Nat. Rev. Cancer *15*, 276–289.
51. Lin, Y.-L., and Pasero, P. (2021). Replication stress: from chromatin to immunity and beyond. Curr. Opin. Genet. Dev. *71*, 136–142.
52. Shiu, J.L., Wu, C.K., Chang, S.B., Sun, Y.J., Chen, Y.J., Lai, C.C., Chiu, W.T., Chang, W.T., Myung, K., Su, W.P., and Liaw, H. (2020). The HLTF–PARP1 interaction in the progression and stability of damaged replication forks caused by methyl methanesulfonate. Oncogenesis *9*, 104–114.
53. Halazonetis, T.D., Gorgoulis, V.G., and Bartek, J. (2008). An Oncogene-Induced DNA Damage Model for Cancer Development. Science *319*, 1352–1355.
54. Kotova, N., Vare, D., Schultz, N., Gradecka Meesters, D., Stepnik, M., Grawé, J., Helleday, T., and Jenssen, D. (2013). Genotoxicity of alcohol is linked to DNA replication-associated damage and homologous recombination repair. Carcinogenesis *34*, 325–330.
55. Peake, J.D., Noguchi, C., Lin, B., Theriault, A., O'Connor, M., Sheth, S., Tanaka, K., Nakagawa, H., and Noguchi, E. (2021). FANCD2 limits acetaldehyde-induced genomic instability during DNA replication in esophageal keratinocytes. Mol. Oncol. *15*, 3109–3124.
56. Hodskinson, M.R., Bolner, A., Sato, K., Kamimae-Lanning, A.N., Rooijers, K., Witte, M., Mahesh, M., Silhan, J., Petek, M., Williams, D.M., et al. (2020). Alcohol-derived DNA crosslinks are repaired by two distinct mechanisms. Nature *579*, 603–608.
57. Mutreja, K., Krietsch, J., Hess, J., Ursich, S., Berti, M., Roessler, F.K., Zellweger, R., Patra, M., Gasser, G., and Lopes, M. (2018). ATR-Mediated Global Fork Slowing and Reversal Assist Fork Traverse and Prevent Chromosomal Breakage at DNA Interstrand Cross-Links. Cell Rep. *24*, 2629–2642.e5.
58. Homann, N., Jousimies-Somer, H., Jokelainen, K., Heine, R., and Salaspuro, M. (1997). High acetaldehyde levels in saliva after ethanol consumption: methodological aspects and pathogenetic implications. Carcinogenesis *18*, 1739–1743.
59. Salaspuro, V., and Salaspuro, M. (2004). Synergistic effect of alcohol drinking and smoking on in vivo acetaldehyde concentration in saliva. Int. J. Cancer *111*, 480–483.
60. Somyajit, K., Gupta, R., Sedlackova, H., Neelsen, K.J., Ochs, F., Rask, M.B., Choudhary, C., and Lukas, J. (2017). Redox-sensitive alteration of replisome architecture safeguards genome integrity. Science *358*, 797–802.
61. Karimian, A., Ahmadi, Y., and Yousefi, B. (2016). Multiple functions of p21 in cell cycle, apoptosis and transcriptional regulation after DNA damage. DNA Repair *42*, 63–71.
62. Cancer Genome Atlas Network (2015). Comprehensive genomic characterization of head and neck squamous cell carcinomas. Nature *517*, 576–582.
63. van Harten, A.M., Buijze, M., van der Mast, R., Rooimans, M.A., Martens-de Kemp, S.R., Bachas, C., Brink, A., Stigter-van Walsum, M., Wolthuis, R.M.F., and Brakenhoff, R.H. (2019). Targeting the cell cycle in head and neck cancer by Chk1 inhibition: a novel concept of bimodal cell death. Oncogenesis *8*, 38.
64. Sano, D., Xie, T.-X., Ow, T.J., Zhao, M., Pickering, C.R., Zhou, G., Sandulache, V.C., Wheeler, D.A., Gibbs, R.A., Caulin, C., and Myers, J.N. (2011). Disruptive TP53 mutation is associated with aggressive disease characteristics in an orthotopic murine model of oral tongue cancer. Clin. Cancer Res. *17*, 6658–6670.
65. Howarth, D.L., Vacaru, A.M., Tsedensodnom, O., Mormone, E., Nieto, N., Costantini, L.M., Snapp, E.L., and Sadler, K.C. (2012). Alcohol disrupts endoplasmic reticulum function and protein secretion in hepatocytes. Alcohol Clin. Exp. Res. *36*, 14–23.
66. Torres, M., Betts, Z., Scholey, R., Elvin, M., Place, S., Hayes, A., and Dickson, A.J. (2023). Long term culture promotes changes to growth, gene expression, and metabolism in CHO cells that are independent of production stability. Biotechnol. Bioeng. *120*, 2389–2402.
67. Choi, D.H., Oh, S.-Y., Choi, J.K., Lee, K.E., Lee, J.Y., Park, Y.J., Jo, I., and Park, Y.S. (2020). A transcriptomic analysis of serial-cultured, tonsil-derived mesenchymal stem cells reveals decreased integrin α3 protein as a potential biomarker of senescent cells. Stem Cell Res. Ther. *11*, 359.
68. Yu, W., Ma, Y., Shankar, S., and Srivastava, R.K. (2018). Chronic ethanol exposure of human pancreatic normal ductal epithelial cells induces cancer stem cell phenotype through SATB2. J. Cell Mol. Med. *22*, 3920–3928.
69. Liu, R., Sun, F., Armand, L.C., Wu, R., and Xu, C. (2021). Chronic Ethanol Exposure Induces Deleterious Changes in Cardiomyocytes Derived from Human Induced Pluripotent Stem Cells. Stem Cell Rev. Rep. *17*, 2314–2331.
70. Gujral, T.S., Chan, M., Peshkin, L., Sorger, P.K., Kirschner, M.W., and MacBeath, G. (2014). A noncanonical Frizzled2 pathway

regulates epithelial-mesenchymal transition and metastasis. Cell *159*, 844–856.

71. Zhan, T., Rindtorff, N., and Boutros, M. (2017). Wnt signaling in cancer. Oncogene *36*, 1461–1473.
72. Yang, D., Li, Q., Shang, R., Yao, L., Wu, L., Zhang, M., Zhang, L., Xu, M., Lu, Z., Zhou, J., et al. (2020). WNT4 secreted by tumor tissues promotes tumor progression in colorectal cancer by activation of the Wnt/β-catenin signalling pathway. J. Exp. Clin. Cancer Res. *39*, 251.
73. Hyakusoku, H., Sano, D., Takahashi, H., Hatano, T., Isono, Y., Shimada, S., Ito, Y., Myers, J.N., and Oridate, N. (2016). JunB promotes cell invasion, migration and distant metastasis of head and neck squamous cell carcinoma. J. Exp. Clin. Cancer Res. *35*, 6.
74. Li, M., Tian, L., Wang, L., Yao, H., Zhang, J., Lu, J., Sun, Y., Gao, X., Xiao, H., and Liu, M. (2013). Down-regulation of miR-129-5p inhibits growth and induces apoptosis in laryngeal squamous cell carcinoma by targeting APC. PLoS One *8*, e77829.
75. Maier, T., Stoiber, S., Gurnhofer, E., Haas, M., Kenner, L., Heiduschka, G., Kadletz-Wanke, L., and Brkic, F.F. (2023). Inhibition of beta-catenin shows therapeutic potential in head and neck squamous cell carcinoma in vitro. Eur. Arch. Oto-Rhino-Laryngol. *280*, 399–408.
76. Harris, P.S., Michel, C.R., Yun, Y., McGinnis, C.D., Assiri, M.A., Ahmadi, A.R., Sun, Z., Roede, J.R., Burchill, M.A., Orlicky, D.J., et al. (2022). Proteomic analysis of alcohol-associated hepatitis reveals glycoprotein NMB (GPNMB) as a novel hepatic and serum biomarker. Alcohol *99*, 35–48.
77. Arosarena, O.A., dela Cadena, R.A., Denny, M.F., Bryant, E., Barr, E.W., Thorpe, R., and Safadi, F.F. (2016). Osteoactivin promotes migration of oral squamous cell carcinomas. J. Cell. Physiol. *231*, 1761–1770.
78. Manevich, L., Okita, Y., Okano, Y., Sugasawa, T., Kawanishi, K., Poullikkas, T., Dang Cao, L.T.L., Zheng, L., Nakayama, M., Matsumoto, S., et al. (2022). Glycoprotein NMB promotes tumor formation and malignant progression of laryngeal squamous cell carcinoma. Cancer Sci. *113*, 3244–3254.
79. Gao, W., Zhang, Y., Luo, H., Niu, M., Zheng, X., Hu, W., Cui, J., Xue, X., Bo, Y., Dai, F., et al. (2020). Targeting SKA3 suppresses the proliferation and chemoresistance of laryngeal squamous cell carcinoma via impairing PLK1-AKT axis-mediated glycolysis. Cell Death Dis. *11*, 919.
80. Kar, N., Gupta, D., and Bellare, J. (2021). Ethanol affects fibroblast behavior differentially at low and high doses: A comprehensive, dose-response evaluation. Toxicol Rep *8*, 1054–1066.
81. Carvalho, L.F.C.S., dos Santos, L., Bonnier, F., O'Callaghan, K., O'Sullivan, J., Flint, S., Neto, L.P.M., Martin, A.A., Lyng, F.M., and Byrne, H.J. (2020). Can ethanol affect the cell structure? A dynamic molecular and Raman spectroscopy study. Photodiagnosis Photodyn. Ther. *30*, 101675.
82. Chi, Z., and Arneborg, N. (1999). Relationship between lipid composition, frequency of ethanol-induced respiratory deficient mutants, and ethanol tolerance in Saccharomyces cerevisiae. J. Appl. Microbiol. *86*, 1047–1052.
83. Avrahami-Moyal, L., Engelberg, D., Wenger, J.W., Sherlock, G., and Braun, S. (2012). Turbidostat culture of Saccharomyces cerevisiae W303-1A under selective pressure elicited by ethanol selects for mutations in SSD1 and UTH1. FEMS Yeast Res. *12*, 521–533.
84. Dal Maso, L., Torelli, N., Biancotto, E., Di Maso, M., Gini, A., Franchin, G., Levi, F., La Vecchia, C., Serraino, D., and Polesel, J. (2016). Combined effect of tobacco smoking and alcohol drinking in the risk of head and neck cancers: a re-analysis of case–control studies using bi-dimensional spline models. Eur. J. Epidemiol. *31*, 385–393.
85. Du, X., Squier, C.A., Kremer, M.J., and Wertz, P.W. (2000). Penetration of N-nitrosonornicotine (NNN) across oral mucosa in the presence of ethanol and nicotine. J. Oral Pathol. Med. *29*, 80–85.
86. Alexandrov, L.B., Kim, J., Haradhvala, N.J., Huang, M.N., Tian Ng, A.W., Wu, Y., Boot, A., Covington, K.R., Gordenin, D.A., Bergstrom, E.N., et al. (2020). The repertoire of mutational signatures in human cancer. Nature *578*, 94–101.
87. Yang, N.J., and Hinner, M.J. (2015). Getting across the cell membrane: an overview for small molecules, peptides, and proteins. Methods Mol. Biol. *1266*, 29–53.
88. Lee, S.H., Samuels, T., Bock, J.M., Blumin, J.H., and Johnston, N. (2015). Establishment of an immortalized laryngeal posterior commissure cell line as a tool for reflux research. Laryngoscope *125*, E73–E77.
89. Harada, H., Nakagawa, H., Oyama, K., Takaoka, M., Andl, C.D., Jacobmeier, B., von Werder, A., Enders, G.H., Opitz, O.G., and Rustgi, A.K. (2003). Telomerase Induces Immortalization of Human Esophageal Keratinocytes Without p16INK4a Inactivation1. Mol. Cancer Res. *1*, 729–738.
90. Gioanni, J., Fischel, J.L., Lambert, J.C., Demard, F., Mazeau, C., Zanghellini, E., Ettore, F., Formento, P., Chauvel, P., Lalanne, C.M., et al. (1988). Two new human tumor cell lines derived from squamous cell carcinomas of the tongue: Establishment, characterization and response to cytotoxic treatment. Eur. J. Cancer Clin. Oncol. *24*, 1445–1455.
91. Weichselbaum, R., Dahlberg, W., Little, J.B., Ervin, T.J., Miller, D., Hellman, S., and Rheinwald, J.G. (1984). Cellular X-ray repair parameters of early passage squamous cell carcinoma lines derived from patients with known responses to radiotherapy. Br. J. Cancer *49*, 595–601.
92. Schneider, C.A., Rasband, W.S., and Eliceiri, K.W. (2012). NIH Image to ImageJ: 25 years of image analysis. Nat. Methods *9*, 671–675.
93. Van Rossum, G., and Drake, F.L., Jr. (1995). Python reference manual (Centrum voor Wiskunde en Informatica Amsterdam).
94. Vichai, V., and Kirtikara, K. (2006). Sulforhodamine B colorimetric assay for cytotoxicity screening. Nat. Protoc. *1*, 1112–1116.
95. Dhar, S., Datta, A., Banerjee, T., and Brosh, R.M. (2019). Single-molecule DNA fiber analyses to characterize replication fork dynamics in living cells. In DNA Repair. Methods in Molecular Biology, L. Balakrishnan and J. Stewart, eds. (Humana Press Inc), pp. 307–318.
96. Mah, L.-J., El-Osta, A., and Karagiannis, T.C. (2010). γH2AX: a sensitive molecular marker of DNA damage and repair. Leukemia *24*, 679–686.
97. Manshian, B.B., Munck, S., Agostinis, P., Himmelreich, U., and Soenen, S.J. (2015). High content analysis at single cell level identifies different cellular responses dependent on nanomaterial concentrations. Sci. Rep. *5*, 13890–13899.
98. Schmittgen, T.D., and Livak, K.J. (2008). Analyzing real-time PCR data by the comparative CT method. Nat. Protoc. *3*, 1101–1108.
99. Ahn, H.R., Baek, G.O., Yoon, M.G., Son, J.A., You, D., Yoon, J.H., Cho, H.J., Kim, S.S., Cheong, J.Y., and Eun, J.W. (2021). HMBS is the most suitable reference gene for RT-qPCR in human HCC tissues and blood samples. Oncol. Lett. *22*, 791.
100. Cutler, K.J., Stringer, C., Lo, T.W., Rappez, L., Stroustrup, N., Brook Peterson, S., Wiggins, P.A., and Mougous, J.D. (2022). Omnipose: a high-precision morphology-independent solution for bacterial cell segmentation. Nat. Methods *19*, 1438–1448.

STAR★METHODS

KEY RESOURCES TABLE

REAGENT or RESOURCE	SOURCE	IDENTIFIER
Antibodies		
Anti-BrdU	BD Biosciences	Cat# 347580; Clone: B44; RRID: AB_400326
Anti-BrdU	Abcam	Cat# ab6326; Clone: BU1/75; RRID: AB_305426
Anti-mouse IgG1 - Alexa 546	Thermo Fisher Scientific	Cat# A-21123; RRID: AB_2535765
Anti-rat - Alexa 488	Thermo Fisher Scientific	Cat# A-11006; RRID: AB_2534074
Anti-phospho-H2AX (Ser139)	Millipore	Cat# 05–636; Clone JBW301; RRID: AB_309864
Anti-mouse - Alexa 488	Cell Signaling Technology	Cat# 4408; RRID: AB_10694704
Anti-Vinculin	Sigma-Aldrich	Cat# V9131; RRID: AB_477629
Anti-ADH7	Abcam	Cat# ab186408; Clone: EPR13949
Anti-Catalase D4P7B XP®	Cell signaling Technology	Cat# 12980; RRID: AB_2798079
Anti-mouse - HRP linked	Cell Signaling Technology	Cat# 7076; RRID: AB_330924
Anti-rabbit - HRP linked	Cell Signaling Technology	Cat# 7074; RRID: AB_2099233
Chemicals, peptides, and recombinant proteins		
Ethanol absolute 99.8%	Acros Organics NV	Cat# E/0650DF
5-iodo-2′-deoxyuridine	Sigma-Aldrich	Cat# I7125
5-chloro-2′-deoxyuridine	MP Biomedicals	Cat# HY-112669
Critical commercial assays		
RNeasy Mini Kit	Qiagen	Cat# 74104
RNase-free DNase Set	Qiagen	Cat# 79254
QuantSeq 3′ mRNA-Seq library prep kit	Lexogen	Cat# 015.96
Deposited data		
Bulk RNA sequencing data	This paper	NCBI: PRJNA989053
Source Data	This paper	Mendeley Data: https://doi.org/10.17632/cfrnv6gj7k.1
Experimental models: Cell lines		
HuLa-PC	ATCC	Cat# CRL-3342™; RRID: CVCL_UC74 Established by Lee et al.[88]
EPC1-hTERT	gift from Prof. H. Nakagawa	Established by Harada et al.[89]
EPC2-hTERT	gift from Prof. H. Nakagawa	Established by Harada et al.[89]
CAL-27	gift from Dr. A. Begg	RRID: CVCL_1107 Established by Gioanni et al.[90]
SCC-61	gift from Dr. A. Begg	RRID: CVCL_7118 Established by Weichselbaum et al.[91]
Oligonucleotides		
Primers for qRT-PCR	Integrated DNA Technologies	Table S1
Software and algorithms		
R version 4.1.1	R Core Team	RRID: SCR_001905 https://www.r-project.org/
STAR version 2.6.0	Dobin et al.[35]	RRID: SCR_004463 https://github.com/alexdobin/STAR
HTSeq	Anders et al.[36]	RRID: SCR_005514 https://github.com/htseq/htseq

(*Continued on next page*)

Continued

REAGENT or RESOURCE	SOURCE	IDENTIFIER
DESEq2 version 1.32.0	R package; Love et al.[38]	RRID: SCR_015687 https://bioconductor.org/packages/release/bioc/html/DESeq2.html
ClusterProfiler v 4.0.5	R package; Wu et al.[41]	RRID: SCR_016884 http://bioconductor.org/packages/release/bioc/html/clusterProfiler.html
ImageJ version 1.52	Schneider et al.[92]	RRID: SCR_003070 https://imagej.net/ij/
Python version 3.10.8	Van Rossum et al.[93]	RRID: SCR_008394 https://www.python.org/
GraphPad Prism 9	Graphpad Software	RRID: SCR_002798 https://www.graphpad.com/

RESOURCE AVAILABILITY

Lead contact

Further information and requests for resources and reagents should be directed to and will be fulfilled by Lead Contact, Prof. Sandra Nuyts.

Materials availability

This study did not generate unique reagents.

Data and code availability

The bulk RNA sequencing data generated in this study have been deposited at NCBI and are publicly available from the date of publication. The accession number is PRJNA989053. The Source Data for all figures and supplementary figures were deposited at Mendeley https://doi.org/10.17632/cfrnv6gj7k.1.

Microscopy data reported in this paper will be shared by the lead contact upon request. Any additional information required to reanalyze the data reported in this paper is available from the lead contact upon request.

No original code was written in preparation for this publication. Existing R packages that were used in this work are listed in the STAR methods and key resources table.

EXPERIMENTAL MODEL AND STUDY PARTICIPANT DETAILS

Cell lines and reagents

The HuLa-PC cell line was purchased from the American Type Culture Collection (ATCC CRL-3342). These cells originated from the posterior commissure of the larynx of a white male patient and were immortalized by the introduction of human papillomavirus E6/E7 genes.[88] These cells were authenticated by short tandem repeats (STR) profiling (see ATCC CRL-3342). HuLa-PC cells were cultivated in fully supplemented Keratinocyte Growth Medium 2 (PromoCell Cat# C-20011). Cells were passaged when 90%–95% confluent and seeded at a density of 8000 cells per cm^2.

EPC1-hTERT and EPC2-hTERT cells were a generous gift from Prof. H. Nakagawa, Herbert Irving Comprehensive Cancer Center (Columbia University, New York, USA). EPC1 and EPC2 primary cells were derived from a 65-year-old and 55-year-old male patient undergoing esophagectomy respectively (Prof. H. Nakagawa personal communication). Both cell lines were derived from a morphologically normal site. These cell lines were immortalized by overexpression of the catalytic subunit of telomerase, hTERT.[89] Both EPC-hTERT cell lines were also authenticated by STR profiling at ATCC (Prof. H. Nakagawa). These cell lines were cultivated in fully supplemented Keratinocyte Growth Medium 2 (PromoCell Cat# C-20011). Cells were passaged when 90%–95% confluent and seeded at a density of 8000 cells per cm^2.

CAL-27 and SCC-61 cell lines were a generous gift from Dr. A. Begg, The Netherlands Cancer Institute Amsterdam. CAL-27 cells were established from an HPV-negative tongue squamous cell carcinoma of a Caucasian male patient.[90] SCC-61 cells were established from an HPV-negative tongue squamous cell carcinoma of a male patient.[91] We authenticated these cancer cell lines by STR profiling at ATCC in 2018. Both cell lines were cultured in Dulbecco's Modified Eagle Medium (Thermo Fisher Scientific Cat# 41965062) supplemented with 1% sodium pyruvate (Life Technologies Cat# 11530396) and 10% Fetal Bovine Serum (Life Technologies Cat# 10270106).

All cell lines were checked every three months to ensure they were mycoplasma free. All cell cultures were propagated in a Binder CO2 incubator controlled at 37°C and 5% CO_2.

METHOD DETAILS

Ethanol treatment

Ethanol absolute 99.8% was purchased from Acros Organics NV (Cat# E/0650DF) and diluted in cell growth medium to reach the appropriate concentrations, as specified in the results section. When cells were exposed for 24 h or longer, culture flasks or dishes were placed in a 'compensation system', as described before.[34] Flasks were place inside a closed polypropylene box with an open pan containing ethanol in aqueous solution. The concentration of ethanol in the open pan was the same as the concentration of ethanol in the cell culture flasks. This compensation system minimized ethanol evaporation during incubation, which we validated by measuring ethanol concentrations by using the Alcolyzer Analyzing System of Anton-Paar (Figure S2B).

Cell survival and proliferation

A sulforhodamine B (SRB) assay was used to assess cell survival and proliferation as described before.[94] Cells were seeded in 96-well plates (Greiner Bio-one Cat# 655180) and were allowed to attach overnight. The next day, the ethanol-containing medium was added and cells were incubated for a specific duration. Thereafter, the ethanol-containing medium was aspirated and replaced by fresh growth medium without ethanol and cells were recovered for three to five days until the control wells, treated with 0 mM ethanol, were 95% confluent. Cells were subsequently fixed by 10% trichloroacetic acid (Merck Millipore Cat# 100807) and stained with 0.4% SRB in 1% acetic acid (Sigma-Aldrich Cat# S1402; VWR Cat# 20104298). The SRB dye was then dissolved by a 10 mM Tris Base solution (Sigma-Aldrich Cat# T1503) and absorbance at 570 nm was quantified by a Multiscan FC spectrophotometer (Thermo Fisher Scientific). SRB binds to the cell's protein content and therefore the absorbance values are proportional to the number of cells in each well.[94] Survival was calculated relative to the control cells, treated with 0 mM ethanol, in every 96-well plate.

$$Relative\ Survival\ (\%) = \frac{N\ treated}{N\ control} * 100$$

With N = the cell density of specific wells.

To quantify population doubling time, we used the SRB assay in a slightly different way. Cells were seeded in 96-well plates (Greiner Bio-one Cat# 655180) and exposed to ethanol. To follow up on the increase in cell density, cells were fixed every day for 5 consecutive days. The population doubling time was calculated in the exponential growth phase, usually between days 2 and 5, as follows:

$$\text{Population doubling time (h)} = T\frac{\ln 2}{\ln\left(\frac{N\ end}{N\ initial}\right)}$$

With T = the duration of the exponential growth phase and N = the cell density at a specific time point.

Bulk RNA sequencing and analysis

HuLa-PC cells were grown in 0, 20, or 250 mM ethanol-containing growth medium for 4 h, 24 h, or 30 days. For the prolonged incubation of 30 days, cells were passaged when they reached 85%–95% confluence. Every culture flask of this experiment was kept in a compensation system where the open pan contained water with 0, 20, or 250 mM ethanol. After incubation, around 1 million cells were harvested and RNA was extracted using the Qiagen RNeasy kit (Qiagen Cat# 74104). For cell lysis, 10 μL β-mercaptoethanol (Sigma-Aldrich Cat# M3148) was added per 1 mL of RLT buffer (part of Qiagen Cat# 74104). We used 350 μL of this lysis buffer for each cell pellet and then 350 μL of 70% ethanol was added to the lysate. This mixture was transferred to an RNeasy Mini spin column (part of Qiagen Cat# 74104) and the sample was centrifuged in a microcentrifuge (Eppendorf 5415R) at 10,000 × g for 30 s. Next, columns were washed once with 350 μL of Buffer RW1 (part of Qiagen Cat# 74104) using the same centrifugation settings. To ensure full DNA removal, we performed on-column DNase digestion with the RNAse-Free DNase Set (Qiagen Cat# 79254). Each sample was incubated with 10 μL DNase I stock solution (part of Qiagen Cat# 79254) in 70 μL RDD Buffer (part of Qiagen Cat# 79254) at room temperature for 15 min. Afterward, 350 μL of Buffer RW1 was directly added to the columns and the columns were centrifuged as before. Lastly, columns were washed twice with 500 μL RPE Buffer (part of Qiagen Cat# 74104) using the same centrifugation settings. The samples were centrifuged once more for 2 min to dry the membranes. Lastly, 30 μL of RNase-free water (part of Qiagen Cat# 74104) was added directly to the column and the tubes were centrifuged at 8000 × g for 1 min to collect the RNA in a fresh collection tube (part of Qiagen Cat# 74104).

RNA samples were prepped for sequencing with the QuantSeq 3′ mRNA-Seq library prep kit (Lexogen Cat# 015.96). These Lexogen QuantSeq 3′ mRNA libraries were sequenced on an Illumina HiSeq4000 generating single-end 51 bp reads. Optical duplicates and adaptors were removed with Clumpify version 38.90 and FASTX-Toolkit version 0.0.14, respectively. Next, the reads were mapped to the human reference genome GrCH38 with STAR version 2.6 and gene-expression matrices were generated with HTSeq version 0.13.5. Every sample had around 3.5 million uniquely mapped reads. Differential gene expression was assessed with DESEq2 version 1.32.0 in R version 4.1.1. Note that this algorithm takes raw counts as input.[38] To account for possible gene expression variation induced by culture time, we only assessed differential gene expression between ethanol-treated and control samples from the same time point. Functional enrichment was performed by Gene Set Enrichment Analysis (GSEA) incorporated in the R package clusterProfiler version 4.0.5. As input for GSEA, we used the entire gene lists sorted according to log2 fold changes, which were derived from DESEq2. We excluded gene ontology categories with less than 15 genes or more than 500 genes, as recommended by.[40] Results were visualized by the treeplot and cnetplot functions embedded in the

R package enrichplot version 1.20.0 (part of clusterProfiler). In detail, we only selected the 30 most significantly enriched GO terms for the treeplots. Clustering was performed by using the Jaccard's similarity index and average linkage.[41] The overarching description of each cluster was manually adapted to better reflect the variety of GO terms in each cluster. It should be noted that there is redundancy in the genes related to different biological processes in one cluster, which results in little additional information of the individual GO terms in each cluster. Subsequently, we also generated gene-concept networks with cnetplot. To improve readability, we limited the number of GO terms and the number of genes shown. The GO terms were selected from the clusters in the treeplots, taking into account the diversity of GO terms. For each of the selected GO terms, only the 15 most up or downregulated genes were visualized. Lastly, heatmaps with selected genes and expression changes in ethanol-treated conditions were generated by using the R package pheatmap version 1.0.12.

Cell cycle analysis

Cells were seeded and cultivated in medium with or without ethanol. At specified time points, cells were harvested, washed with Dulbecco's phosphate-buffered saline (DPBS, Thermo Fisher Scientific Cat# 14190169) and fixed with ice-cold 70% ethanol. To be able to distinguish between cell cycle phases, cells were stained with DPBS containing 10 μg/mL propidium iodide (PI, Sigma-Aldrich Cat# P4170) and 100 μL/mL RNase A (Invitrogen Cat# 12091021). The staining was incubated in the dark for 20 min and cells were subsequently analyzed with a FACSVerse flow cytometer (BD Biosciences) where PI was excited at 488 nm and the emitted fluorescence was detected by a red bandpass filter 586/42. The BD FACSuite software version 1.0.6 was used to analyze the cell cycle profiles. First, gating on forward and side scatter was used to select single cells. Then cell count versus linear fluorescence was plotted to gate for G0/G1, S, and G2/M cell cycle phases.

DNA fiber analysis

The DNA fiber analysis was performed as described before.[95] To follow replication fork progression, the DNA was labeled with two thymidine analogs, 5-iodo-2′-deoxyuridine (IdU, Sigma-Aldrich Cat# I7125) and 5-chloro-2′-deoxyuridine (CldU, MP Biomedicals Cat# HY-112669). Cells were consecutively treated with 20 μM IdU and 80 μM CldU for exactly 30 min. Only during the second pulse labeling with CldU were the cells also treated with MMS (Sigma-Aldrich Cat# 129925) or ethanol. After pulse DNA labeling and treatment, cells were harvested and washed once with DPBS (Thermo Fisher Scientific Cat# 14190169). Subsequently, 2 μL of cell suspension, with a concentration of 1 million cells per mL, was placed on an X72 SuperFrost Plus Adhesion slide (Thermo Fisher Scientific Cat# J1800AMNZ). The cells were lysed by adding 7 μL of spreading buffer, consisting of 200 mM Tris pH 7.5 (Sigma-Aldrich Cat# T1503), 50 mM ethylenediaminetetraacetic acid (EDTA, VWR Cat# ACRO409975000) and 0.5% sodium dodecyl sulfate (SDS, National Diagnostics Cat# EC-874). DNA fibers were spread by tilting the glass slides 45° so the drops could run down to the bottom of the slides. DNA fibers were fixed by submerging the slides in a 3:1 methanol-acetic acid solution (Acros Organics NV Cat# 268280025; VWR Cat# 20104298) at room temperature for 10 min. Slides were air-dried and stored at 4°C until staining. To denature the DNA, slides were submerged in 2.5 M of hydrochloric acid (HCl, Sigma-Aldrich Cat# 100314) rocking gently at room temperature for 1 h. After washing the slides with DPBS three times, blocking was performed with DPBS containing 0.1% Tween 20 (VWR Cat# 822184) and 1% Bovine Serum Albumin (BSA, Sigma-Aldrich Cat# A9647). Staining was performed with the primary antibodies anti-BrdU clone B44 and anti-BrdU clone BU1/75, diluted 1:250 in blocking buffer, followed by staining with the secondary antibodies anti-Mouse Alexa 546 and anti-Rat Alexa 488, diluted 1:100 in blocking buffer (details antibodies in key resources table). For each slide, 50 μL of antibody solution was used and slides were incubated at 37°C for 30–45 min. In between primary and secondary antibody staining, the slides were washed three times with DPBS containing 0.1% Tween 20. Lastly, 30 μL ProlongGold (Thermo Fisher Scientific Cat# P10144) was used to mount the slides and slides were stored in the dark until imaging. Immunofluorescence images were acquired with an Olympus BX43 microscope equipped with Olympus XM10 and UC30 CCD cameras in combination with a 40x objective. Images were saved in the CellSens software version 1.18 but were further analyzed in ImageJ version 1.52. The IdU track length served as an internal control to correct for differences in DNA spreading. Therefore, the ratio IdU/CldU track length was calculated and statistically compared between different treatment conditions.

Immunofluorescence to detect DNA damage

We used the phosphorylation of the Ser-139 residue of the histone variant H2AX, forming γ-H2AX, as a molecular marker for the induction of DNA double-strand breaks.[96] Cells were seeded in μClear 96-well plates (Greiner Bio-one Cat# 655090) and treated with different concentrations of ethanol for specific times. Afterward, cells were fixed with 4% paraformaldehyde (Acros Organics Cat# 119690010) and permeabilized with 0.3% Triton X-100 (Sigma-Aldrich Cat# T8787) in DPBS (Thermo Fisher Scientific Cat# 14190169) containing 0.5% BSA (Sigma-Aldrich Cat# A9647). Blocking was performed with DPBS containing 1% BSA shaking gently at room temperature for 45 min. Cells were stained with the primary antibody against phosho-H2AX Ser139, dissolved at 1:50 in blocking buffer, followed by staining with the secondary antibody anti-Mouse Alexa 488, dissolved at 1:500 dilution in blocking buffer (details antibodies in key resources table). For each step, 50 μL of antibody solution was added to every well and plates were incubated at room temperature for 1 h. Nuclei were counterstained with 1 μL/mL 4′,6-diamidino-2-phenylindole (DAPI, Sigma-Aldrich Cat# D9542). Immunofluorescence images were acquired with an Operetta CLS LIVE high-content analysis system equipped with a large format CMOS camera in combination with a 20x air NA 1.0 objective. Images were analyzed by the Harmony Software version 4.9 (PerkinElmer). The DAPI staining was used to segment the images and then green fluorescent spots were identified by method D in the Harmony software. The average number of green foci per cell was calculated for each condition and each biological replicate.

For CAL-27 and SCC-61, immunofluorescence images were acquired with In Cell analyzer 2000 with a 40x objective (GE Healthcare Life Sciences). Data analysis was then performed on the InCell Investigator software (GE Healthcare Life Sciences). The DAPI staining was used to perform nuclear segmentation and then green fluorescent foci were identified based on areas of 1–4 μm^2 where the green fluorescent intensity was minimally 2-fold above the background level.

Quantification of intracellular reactive oxygen species

To assess oxidative stress in cells exposed to ethanol, levels of intracellular reactive oxygen species (ROS) were quantified as described in detail before.[97] Cells were seeded in μClear 96-well plates (Greiner Bio-one Cat# 655090) and treated with ethanol after overnight attachment. After incubation in ethanol, 5 μM CellROX Green (Thermo Fisher Scientific Cat# C10444) was added and plates were incubated at 37°C for 30 min. Next, cells were fixed with 4% paraformaldehyde and nuclei were counterstained with 1 μg/mL DAPI. Image acquisition was performed with the InCell 2000 high-content imaging system (GE Healthcare Life Sciences). We analyzed the images with the InCell Investigator software version 1.5 as described by Manshian et al.[97] The percentage of ROS-positive cells was calculated as follows: First, cell nuclei were segmented based on the blue channel which corresponds to the DAPI staining. "As CellROX Green localizes in the nucleus upon oxidation, the intensity of light emitted in the green channel was then determined for every area of the corresponding nuclei. The intensity of every nucleus was then calculated for the green channel".[97] Based on a cut-off value on fluorescence intensity, the percentage of ROS-positive cells was calculated. This cut-off was cell line dependent and was determined by using a value where more than 50% of the positive control cells were positive. For HuLa-PC cells this value was 120 a.u.

Transient gene knockdown

To transiently inhibit the expression of ethanol metabolizing genes, we used RNA interference. We purchased an *ADH7*-targeted siPOOL from siTOOLs Biotech which contained 30 selected small interfering RNAs (siRNAs). An untargeted siPOOL with sequences not found in humans, mice, or rats was used as a negative control. To also inhibit the expression of *CAT*, we combined these siPOOLs with predesigned Dicer-Substrate Short Interfering RNAs (DsiRNAs) from Integrated DNA Technologies (IDT). The untargeted siPOOL was combined with the untargeted DsiRNA (IDT Cat# 51-01-14-03). The *ADH7*-targeted siPOOL was combined with *CAT*-targeted DsiRNA (IDT Cat# hs.Ri.CAT.13.1). All oligonucleotides were used in 3 nM final concentration. To introduce the RNA molecules, the Lipofectamine 3000 transfection reagent (Invitrogen Cat# L3000001) was used at 1:600 final dilution. Both the oligonucleotides and Lipofectamine 3000 were first diluted in opti-MEM (Thermo Fisher Scientific Cat# 31985062). Then the diluted oligonucleotides were added to the tubes with diluted Lipofectamine 3000 in a 1:1 ratio. These tubes were incubated at room temperature for 15 min after which the RNA-lipid complexes were added to adherent cells. Transfection was performed for 24 h whereafter cells were analyzed or seeded again for assays to determine the effect of ethanol as described before. The transfection efficiency as assessed by transfection with the BLOCK-iT Fluorescent Oligo (Thermo Fisher Scientific Cat# 2013) was around 80% (Figure S15).

RNA isolation, cDNA synthesis, quantitative reverse-transcription polymerase chain reaction (qRT-PCR)

RNA was isolated from cell pellets by using the Qiagen RNeasy kit (Qiagen Cat# 74104) according to the description given in the RNA sequencing section above. The concentration of RNA was determined by assessing absorbance at 260 nm with a Nanodrop2000 (Thermo Fisher Scientific). Subsequently, cDNA synthesis was performed on 0.5–1 μg of total RNA with the SuperScript VILO cDNA synthesis kit (Thermo Fisher Scientific Cat# 11754050). In short, the RNA samples were mixed with 2 μL 10X SuperScript Enzyme Mix, 4 μL 5X VILO Reaction Mix, and DEPC water (Thermo Fisher Scientific Cat# AM9915G) to a total volume of 10 μL. Samples were then incubated in a ProFlex PCR System (Life Technologies) using the following protocol: 25°C for 10 min, 42°C for 60 min, and 85°C for 5 min. For qRT-PCR, all cDNA samples were first diluted to 4 ng/μL in DEPC water (Thermo Fisher Scientific Cat# AM9915G). Then 5 μL of cDNA samples was mixed with 7.5 μL of LightCycler 480 SYBR Green I Master mix (Roche Cat# 4707516001) and 1.25 μL of both forward and reverse primers at 5 μM concentration. The primers that were used to detect the different genes are depicted in Table S1. All primers were purchased from IDT and dissolved in nuclease-free DEPC water. qRT-PCR samples were analyzed in technical duplicate in a CFX Connect Real-Time PCR Detection System (Bio-Rad). PCR conditions consisted of an initial activation at 95°C for 10 min, followed by 40 amplification cycles of 95°C for 10 s and 60°C for 30 s. Green fluorescence was acquired at the end of every amplification cycle.

Quantification of the threshold cycle (Ct) values was done by regression in the Bio-Rad CFX Manager software version 3.1. Calculation of relative expression was done by the delta-delta Ct method as described before.[98] We used the average of the expression of two housekeeping genes, *HPRT*1 and *HMBS*,[99] as an internal control to normalize the expression values.

$$Relative\ expression = 2^{-[(Ct\ gene\ of\ interest - Ct\ internal\ control)A - (Ct\ gene\ of\ interest - Ct\ internal\ control)B]}$$

With A and B two separate samples. For these knockdown experiments, sample A corresponded to a transfected sample while sample B corresponded to the not transfected control.

Immunoblotting

To confirm transient knockdown on the protein level, Western blots were performed. Cells were harvested after transfection and proteins were extracted with a RIPA buffer which consisted of 150 mM sodium chloride (Thermo Fisher Scientific Cat# S/3160/60), 1% Triton X-100

(Sigma-Aldrich Cat# T8787), 0.5% sodium deoxycholate (Sigma-Aldrich Cat# D6750), 0.1% SDS (National Diagnostics Cat# EC-874) in 50 mM Tris pH 8.0 (Sigma-Aldrich Cat# T1503). The RIPA buffer did also contain the Roche protease inhibitor cocktail (Sigma-Aldrich Cat# 4693116001) and a 200 mM sodium orthovanadate phosphatase inhibitor (Sigma-Aldrich Cat# S6508). Cells were lysed on ice for 30 min and lysates were clarified by centrifugation at 16,000 × g for 20 min. The supernatant, containing the proteins, was transferred to a clean tube and stored at −20°C until further processing. Protein concentrations were determined using the Bradford reagent (Bio-rad Cat# 5000006) and a standard of BSA (Sigma-Aldrich Cat# A9647). Samples were diluted 1:1000 in the Bradford reagent and the absorbance was measured at 595 nm with a UVmini-1240 Model Spectrophotometer (Shimadzu). For each sample, 10 μg of proteins were reduced and denatured by mixing with 2.5 μL NuPAGE LDS Sample Buffer 4x (Invitrogen Cat# NP0007), 1 μL NuPAGE Sample Reducing Agent 10x (Invitrogen Cat# NP0004), and RIPA lysis buffer to 10 μL and thereafter incubating at 70°C for 10 min. To separate proteins, the denatured and reduced samples were loaded onto a NuPAGE 4%–12% Bis-Tris (Invitrogen Cat# NP0323BOX) and gel electrophoresis was performed in the NuPAGE MOPS SDS running buffer (Invitrogen Cat# NP0001). The SeeBlue Plus2 Pre-stained Protein Standard (Thermo Fisher Scientific Cat# LC5925) was used as a ladder. Afterward, proteins were transferred to a PVDF membrane by semi-dry transfer in a Trans-Blot Turbo Transfer System (Bio-Rad) set at 25 V for 30 min. The PVDF membrane was first activated by consecutively submerging it in methanol (Acros Organics NV Cat# 268280025), demi water, and transfer buffer for 30 s. The transfer buffer was a solution of 25 mM Tris with 192 mM glycine (Acros Organics Cat# AC220910010) and 20% methanol. After transfer, blocking was performed with a blocking buffer consisting of 5% non-fat dry milk (VWR Cat# A0830) in TBS-T buffer, i.e., Tris-Buffered Saline, i.e., 20 mM Tris pH 7.6 with 150 mM sodium chloride (Thermo Fisher Scientific Cat# S/3160/60) and 2% Tween 20 (VWR Cat# 822184). Next, blots were incubated with primary antibodies, dissolved 1:1000 in blocking buffer, shaking gently at 4°C overnight. The following primary antibodies were used: anti-Vinculin, anti-*ADH7*, and anti-Catalase (details key resources table). The next day, blots were washed three times with TBS-T which was followed by the incubation with the secondary anti-mouse and anti-rabbit antibodies linked to Horseradish Peroxidase (HRP, details key resources table), dissolved 1:3000 in blocking buffer, shaking gently at room temperature for 1 h. Protein bands were detected by using enhanced chemiluminescence (ECL, PerkinElmer Cat# NEL112001EA) and visualized with an AI680 Western blot imager (GE Healthcare). Densitometry was performed via ImageJ version 1.52. The protein signals were normalized to the signal of the loading control, i.e., vinculin, in each sample.

Analysis of cell morphology

HuLa-PC cells were grown in medium with or without 250 mM ethanol for 48 h. Subsequently, bright field images were acquired at 10x magnification with an Olympus IX71 microscope equipped with a HAMAMATSU ORCA-spark digital CMOS camera (Model C11440-36U). Image analysis was performed in ImageJ and Python. First, images were pre-processed with a bandpass filter (hyperparameters: 30, 1, 3) to enhance contrast. Second, segmentation of the resulting images was performed in Python using the Omnipose algorithm with the cyto2 model.[100] From the obtained cell masks, two features were extracted, the area and the aspect ratio. The area corresponds to the cell size (in pixels). The aspect ratio is the major axis of the cell divided by its minor axis and is a measure of a cell's roundness.

QUANTIFICATION AND STATISTICAL ANALYSIS

For statistical analyses, GraphPad Prism Software (version 9) was used. Different statistical tests were used depending on the type of data that was handled. These details are further specified in every figure caption. p-values smaller than 0.05 were considered statistically significant.